— BRIEFING CHARTS —

STUDY FOR AN OPTICAL TECHNOLOGY APOLLO

EXTENSION SYSTEM (OTES)

PERKIN ELMER

PERKIN-ELMER

ELECTRO-OPTICAL DIVISION   NORWALK, CONNECTICUT

LOCKHEED

ENGINEERING REPORT NO. ___8274___

BRIEFING CHARTS FOR THE NASA MEETING AT
PERKIN-ELMER ON THE PROJECT:
STUDY FOR AN OPTICAL TECHNOLOGY APOLLO
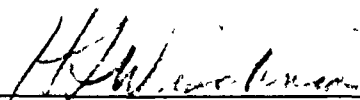EXTENSION SYSTEM (OTES)

DATE ___JANUARY 18, 1966___

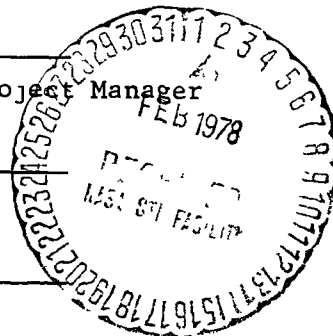PREPARED FOR ___MARSHALL SPACE FLIGHT CENTER___

___NATIONAL AERONAUTICS AND SPACE ADMINISTRATION___

___HUNTSVILLE, ALABAMA___

CONTRACT NAS 8-20255

Herbert F. Wischnia, OTES Project Manager

THE OPTICAL TECHNOLOGY EXPERIMENT SYSTEM MEETING
AT THE PERKIN-ELMER CORPORATION ON JANUARY 18, 1966

TIME	NO.	EVENT	SPEAKER
8:45-9:00 AM	1.	The OTES Project and the Project Objectives (Figure 1)	H.F. Wischnia, Project Manager, OTES
9:00-9:30	2.	The 1980 Space Telescope	R.M. Scott, V.P., Chief Scientist, P-E
9:30-9:45	3.	Space Optics and Perkin-Elmer	C.W. Nimitz, Jr., Pres. Perkin-Elmer Corporation
9:45-10:00	4.	Informal Discussion	
10:00-10:30	5.	Study Areas and Some Important Candidate Experiments (Figures 2, 3, 4)	H.F. Wischnia
10:30-11:15	6.	Pointing Considerations and Associated Experiments Pointing 1/10 and 1/100 Arc Second Suspensions Comparison and Pointing Disturbances (Figures 5-17)	E.R. Schlesinger, Senior Staff Engineer
11:15-11:30	7.	Space Optical Systems and Techniques Laser/Optics Techniques Active Optics (Figures 18, 19)	H.S. Hemstreet, Manager, Space Optics Department
11:30-12:15	8.	Laboratory Demonstrations in Space Optics Laser/Optics Technique Program	M.S. Lipsett, Project Manager, Laser/Optics Techniques
		Laser Transmitter/Receiver Isolation (Figures 20, 21)	S. Habijanec, Senior Physicist
		In-Flight Alignment of Optical Systems (Figure 22)	M.S. Lipsett
		Active Optics Program Phase Measuring Interferometer for $\lambda/50$ Figure Sensing (Figures 23, 24)	H. Robertson, Project Manager, Active Optics

| TIME	NO.	EVENT	SPEAKER
	8. Cont.	Actuators for Active Optics (Figures 29-32)	H. Robertson
		White-Light Interferometer for Figure Sensor (Figures 25-28)	R. Crane, Senior Staff Engineer
1:00-1:15	9.	Systematic Search for Prospective Space Experiments in Optical Technology (Figure 33)	H.F. Wischnia
1:15-2:00	10.	AES Spacecraft for a Three-Meter Aperture OTES Concept Principal Problem Areas Operational Sequence Stored Configuration Concept Advantages (Figures 34-38)	W. Mimnaugh, LMSC, OTES, Project Manager
2:00-2:30	11.	CO_2, Argon, Helium-Neon and Other Gas Lasers Today and Tomorrow (Figures 39-42)	J.D. Rigden, Senior Staff Physicist
2:30-3:30	12.	Laser Communication Experiments Point Ahead Station Transfer Communications Considerations CO_2 versus He-Ne (Figures 43, 44, 45)	W. Peters, Engineer
		Heterodyning on Earth	R. Arguello, Senior Staff Engineer
		Atmospheric Scintillation (Figures 46-52)	R. Arguello
3:30-4:15	13.	NASA Discussion	

NATIONAL AERONAUTICS AND SPACE ADMINISTRATION ATTENDEES AT THE
OPTICAL TECHNOLOGY EXPERIMENT SYSTEM MEETING

C. Dixon Ashworth	OSSA
Roland Chase	OAR & T
Norman S. Johnson	ARC
Edwin P. Martz	JPL
Dr. Duncan E. McIver, Jr.	LRC
Dr. Max R. Nagel	ERC
Dr. Henry H. Plotkin	GSFC
Dr. Joseph L. Randall	MSFC
Earl J. Reinbolt	MSFC
Dr. Nancy G. Roman	OSSA
A. R. Sinclair	LRC
Conrad D. Swanson	MSFC
Dr. James C. Taylor	MSFC
W. L. Thompson	MSC
Hubert Tschunko	ERC
Dr. John M. Walker	OAR & T
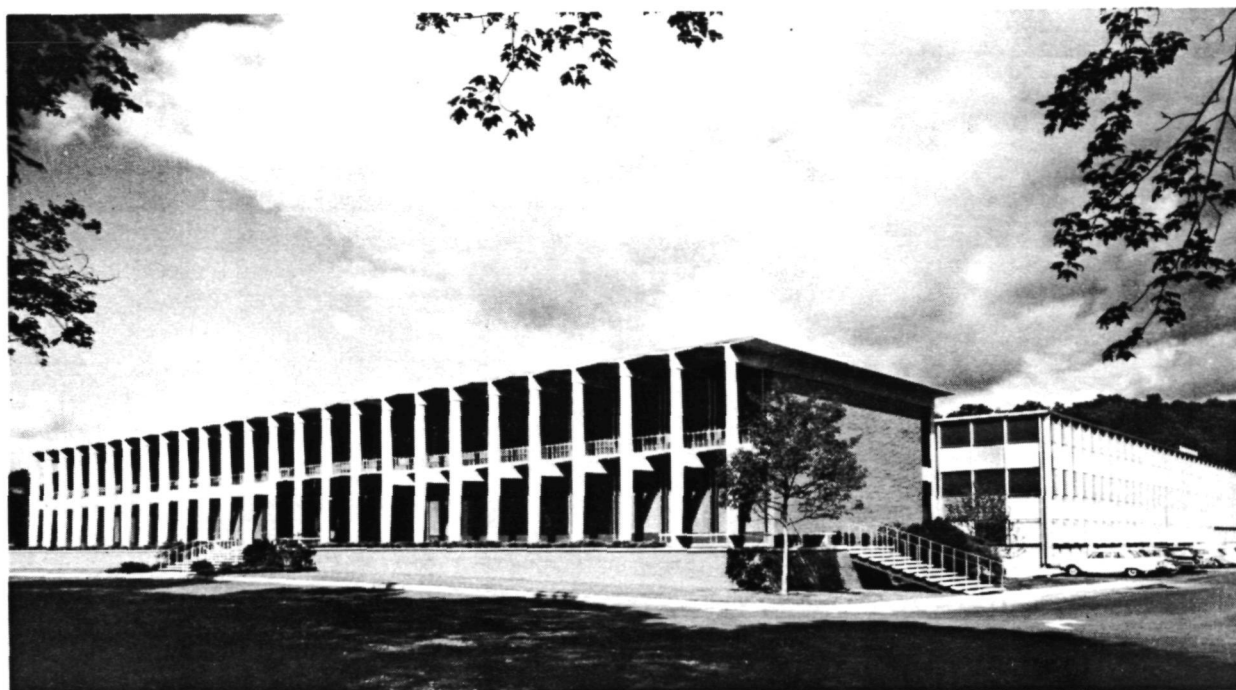
The Perkin-Elmer Corporation - Site of the OTES Meeting

PHASE I - JUSTIFICATION of WORTHWHILE OPTICAL EXPERIMENTS

TEST I - WILL THE EXPERIMENT PROVIDE AN ANSWER TO A KEY
ENGINEERING QUESTION IN THE DEVELOPMENT of
SPACE OPTICS ?

TEST 2. - IS IT TECHNICALLY MORE DIFFICULT (OR EVEN IMPOSSIBLE)
TO CONDUCT THE EXPERIMENT ON EARTH ?

TEST 3. - WILL THE EXPERIMENT PROVIDE ANSWERS TO IMPORTANT
SCIENTIFIC QUESTIONS ?

PHASE II - FEASIBILITY of EXPERIMENTS

COMPLETE SYSTEM CONCEPTS

ANALYSIS AND DOCUMENTATION TO
SUPPORT RECOMMENDATIONS

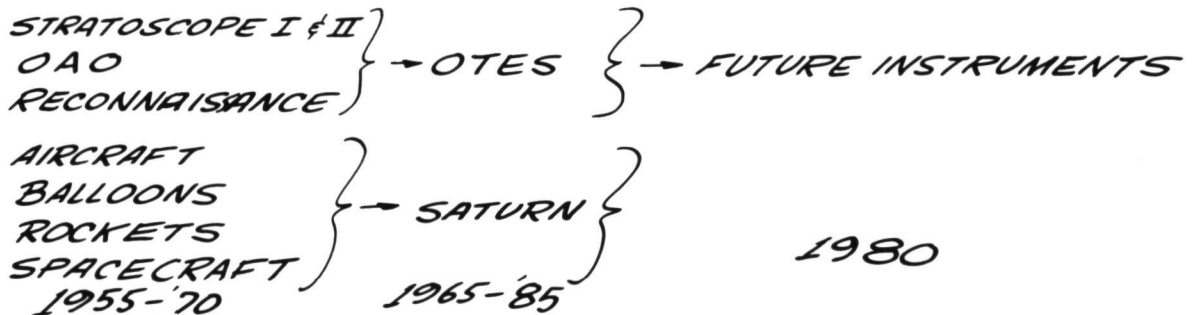Figure 1. OTES Project Objectives

1. BROAD BASED CANDIDATE EXPERIMENTS

(a) WHAT ARE THE FUTURE NEEDS of SPACE OPTICAL TECHNOLOGY?

(b) WHAT EXPERIMENTS COULD BE DONE ON A SATELLITE?

2. IMPORTANT EXPERIMENTS

(a) EXPERIMENT REVIEW BOARD:

    J.G. ATWOOD, Chairman   Prof. M. SCHWARZCHILD

    Dr. A. MEINEL   Mr. L. TILLOTSON

(b) ENGINEERING NEEDS FOR SPACE ASTRONOMY

STRATOSCOPE I & II
OAO
RECONNAISANCE
} → OTES { → FUTURE INSTRUMENTS

AIRCRAFT
BALLOONS
ROCKETS
SPACECRAFT
1955-'70
} → SATURN {
1965-'85
    1980

3. ENGINEERING WORK IN PROGRESS

(a) SCALING LAWS   (d) MAN CAPABILITIES

(b) POINTING LIMITS   (e) AES CAPABILITIES

(c) LASER COMMUNICATION SYSTEM   (f) SPACECRAFT CONCEPTS

Figure 2. Current Areas of Study

    This chart identifies the Perkin-Elmer search activity for optical experiments which must be conducted from a satellite. The Perkin-Elmer Experiment Review Board has been established to review experiments recommended by the OTES Project Team.

*1. MIRROR FIGURE MEASUREMENT
ON EARTH USING LASER*

2. ACTIVE OPTICS

*3. TELESCOPE POINTING PRECISION
∠ 1/100 ARC-SECOND*

4. 3 METER APERTURE

5. MEGABIT LASER COMMUNICATION

6. 1/10 ARC-SECOND TRACKING

7. ACQUISITION

8. POINT AHEAD

9. STATION TRANSFER

10. RLOS

Figure 3. Important OTES Experiments

Ten important experiments were described. The value of Mirror Figure Measurement on Earth Using the Laser (Experiment #1) was discussed using Figure 4 (next page). The Active Optics Experiment was described (See Figure 5). The differences between 1/100 arc second Pointing Experiment (Experiment #3) and the 1/10 arc second Pointing Experiment (Experiment #6) are due to the difference between astronomy applications and deep space laser communications applications.

The Three-Meter Aperture Telescope (Experiment #4) is a candidate experiment which could be used to demonstrate the Active Optics (Experiment #2). The Three-Meter Aperture Telescope can also be used for infrared astronomy with the active optics segments deactivated.

The proposed Three-Meter Aperture Telescope can fit into a Saturn V (See Figures 34 through 38). This experiment would be a bold step forward in Space Optics. The rational for the choice of aperture diameter is quite simple: the diameter is large enough to be a significant technical achievement and yet small enough to be accomplished within a reasonable period of time.

The Megabit Laser Communication, Acquisition, Point Ahead, Station Transfer, and RLOS Experiments (Experiments #5,7,8,9, and 10) are optical communication oriented experiments and were justified from an engineering point of view. An operational deep space laser communicator would be required to perform the functions identified; therefore, experiments based on these functions are of value.
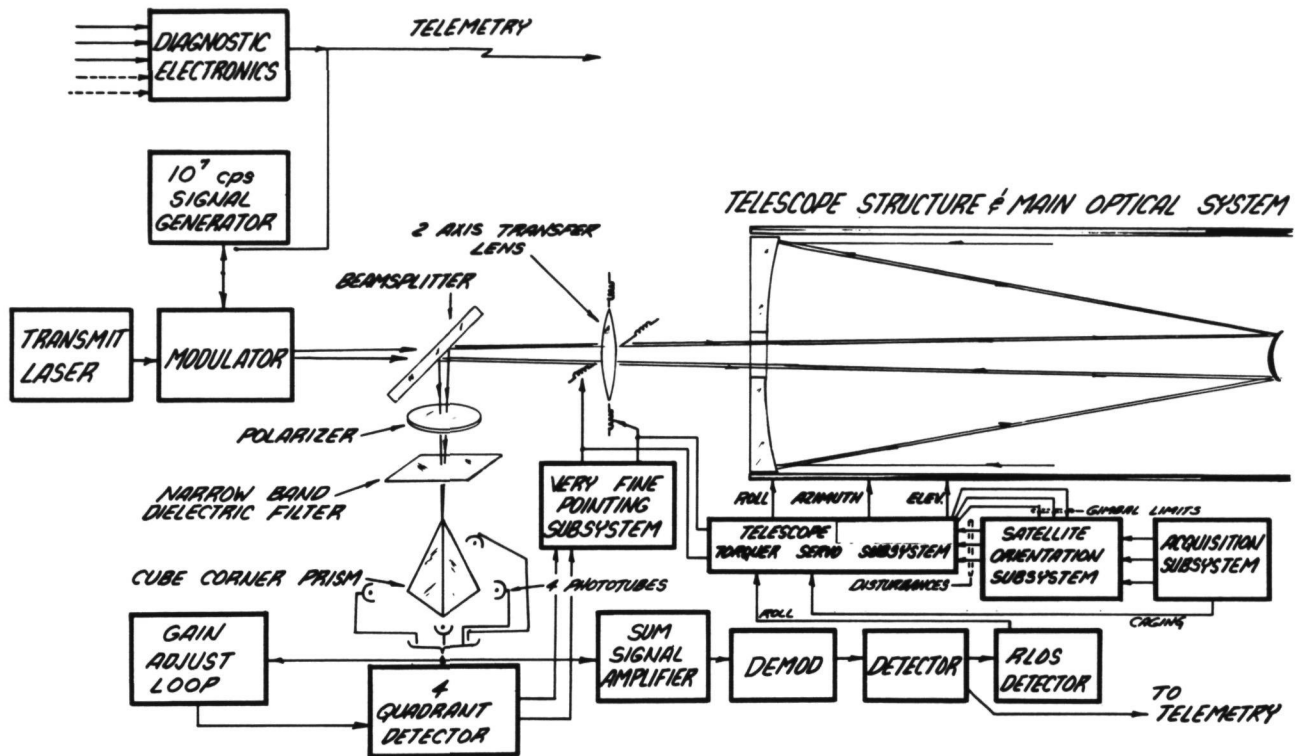
Figure 4. Simplified Block Diagram of a Space Optical Communicator

POINTING EXPERIMENTS

I. DEMONSTRATE ABILITY TO ACQUIRE TARGETS

2. EVALUATE POINTING ACCURACY

3. DETERMINE EFFECTS OF TORQUE DISTURBANCES ON POINTING PERFORMANCE

4. COMPARE POINTING PERFORMANCE OBTAINED WITH ALTERNATE SUSPENSION SYSTEMS

5. DEMONSTRATE POINT-AHEAD CAPABILITY

Figure 5. Five Candidate Pointing Experiments

$$E_{P_{min}} = \frac{1.22\,\lambda}{2D} \left(\frac{S}{N}\right)^{-1} \qquad S/N \gg 1$$

Where λ = WAVELENGTH

D = APERTURE DIAMETER

$S \propto$ MEAN ERROR VOLTAGE AT MAX ERROR

$N \propto$ RMS NOISE VOLTAGE CONTENT IN S
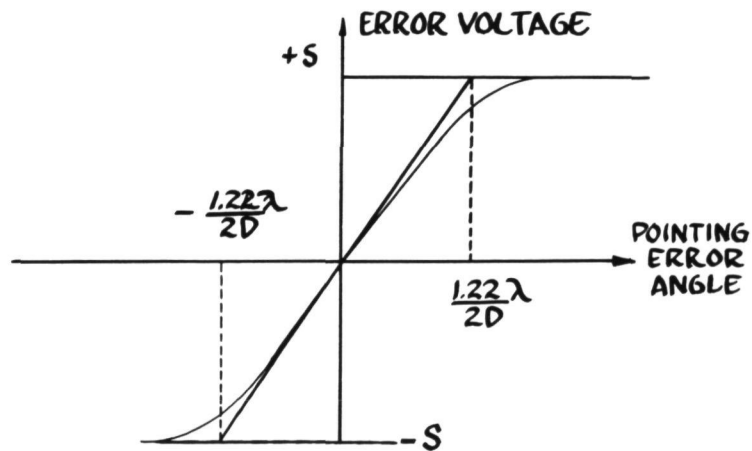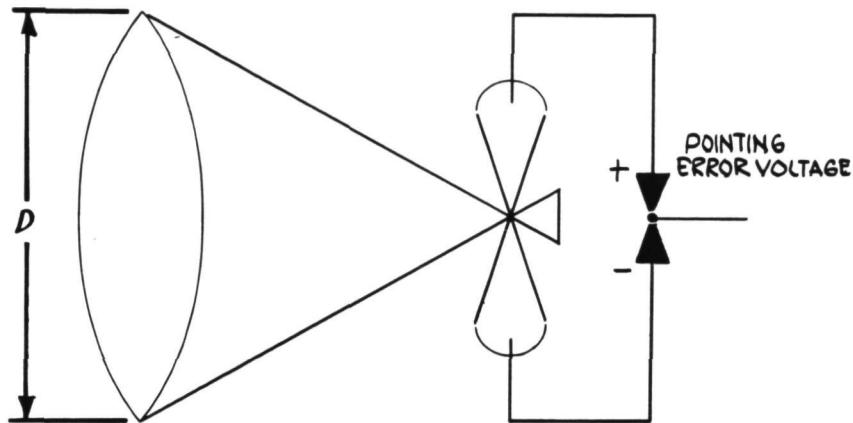
Figure 6.   Image Splitting Techniques

Image splitting techniques can furnish pointing error signals useful in controlling the telescope's line of sight.   In a diffraction-limited instrument, the rms angular pointing error is approximately related to the sensor signal-to-noise ratio and the optical resolution.   This result is applicable whether the image is that of a star or a laser source.

ASTRONOMICAL TELESCOPE

$$Ep_{min} = \frac{1.22}{2D} \lambda \left(\frac{S}{N}\right)^{-1}$$

$$\frac{S}{N} \gg 1$$

$$\frac{S}{N} = \frac{P_s N_o N_Q \Delta t}{\sqrt{(P_s N_o N_Q + E_n)\Delta t}} = \sqrt{\frac{10^{10}}{2.51^{m_v}} \frac{\pi}{4} D^2 N_o N_Q \frac{1}{2\Delta f}}$$

$$Ep_{min} = \frac{K_1}{D^2} \sqrt{\frac{2.51^{m_v} \Delta f}{N_o N_Q}}$$

$$E_{pread} = \frac{1.22 \lambda}{K_2 D} \qquad K_2 > 1$$

$$\text{Pointing Sensor} \atop \text{Figure of Merit} = \frac{E_{pread}}{Ep_{min}} \propto \frac{D}{\sqrt{2.51^{m_v} \Delta f}}$$

Figure 7. Pointing Figure of Merit

The signal-to-noise ratio, in the case of a stellar image, is a function of visual magnitude M_V, optical and quantum efficiencies N_O and N_Q, servo bandwidth, ΔF, etc. As diameter increases, minimum pointing error reduces in square law fashion while the required pointing error reduces linearly. Hence, the system's figure of merit tends to increase with diameter if visual magnitude and bandwidth remain constant.

TWO MIRROR APLANATIC RITCHEY-CHRETIEN ARRANGEMENT

PRIMARY
(PARABOLOID)

IMAGE PLANE

D

SECONDARY
(HYPERBOLOID)
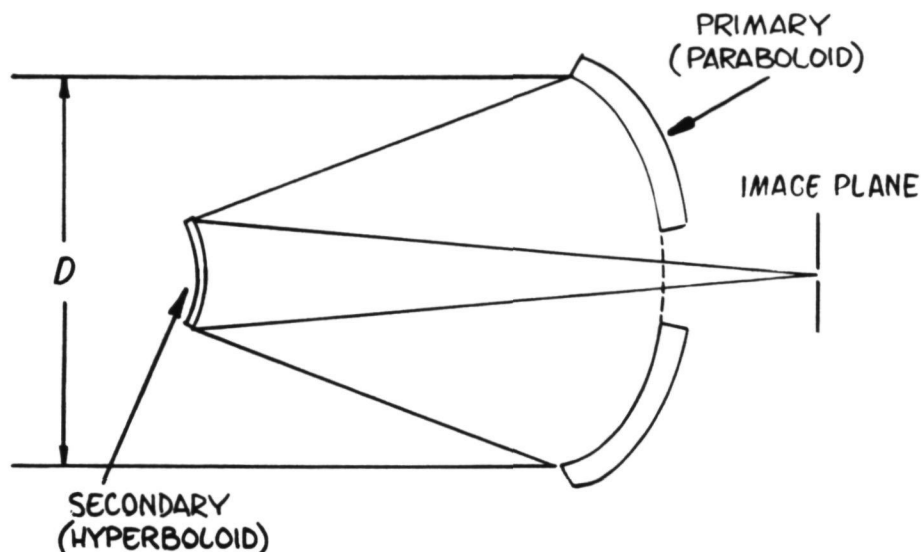
SPHERICAL ABERRATION	ZERO	
COMA	ZERO	
ASTIGMATISM	NON-ZERO	IF (FOV)^{2}D REMAINS CONSTANT WITH SCALING, IMAGE DEGRADATION REMAINS SAME
FIELD CURVATURE	NON-ZERO	
DISTORTION	NO POINT IMAGE DEGRADATION	

Figure 8. Two-Mirror Ritchey-Chretien Arrangement

Visual magnitude may not remain constant as a particular system
is increased in size. Optical aberrations which can cause degraded perfor-
mance may require a reduced field of view. Practical considerations may
dictate that visual magnitude be changed as a particular type of optical
arrangement is increased in size. An Aplanatic Ritchey-Chretien two-mirror
system must have its usable field of view reduced as size is increased to
maintain a constant pointing degradation due to optical aberrations.

FOV TO ENSURE 90% PROBABILITY
OF AT LEAST ONE GUIDE STAR OR
MAGNITUDE M_V OR BRIGHTER
AT GALACTIC POLES

Visual
Magnitude

13
12
11
10
9
8

FOV (Log scale)

.1°   1°   10°

Aperture
diameter
(log scale)

.1D

1D

10D

100D

$(FOV)^2 D = CONSTANT$

$$\triangle M_V = 5.21 \log N^{1/2}$$

Where N is the factor by
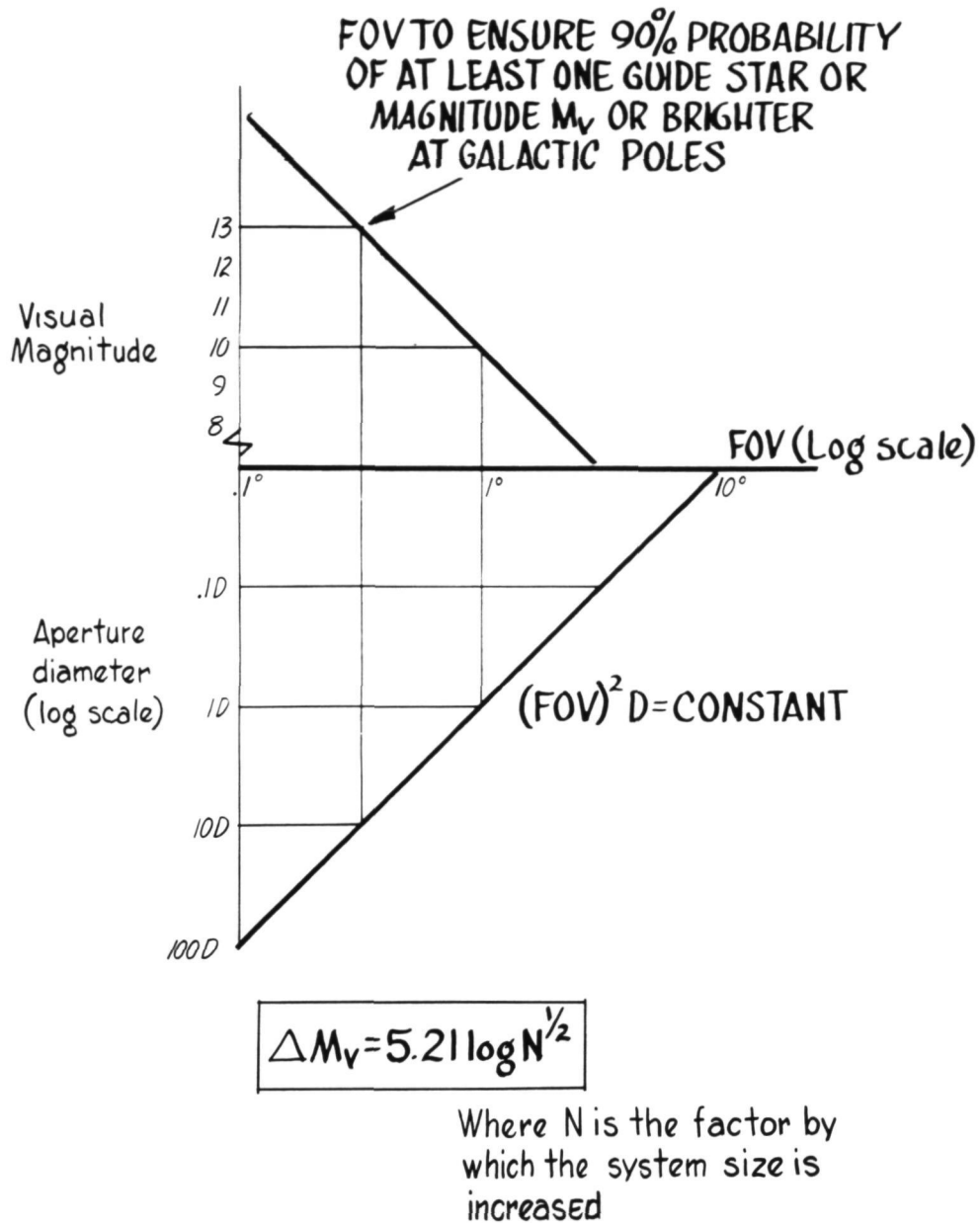which the system size is
increased

Figure 9.   Scaling the Diameter and Its Effect
on Visual Magnitude

Decreasing the allowed field of view with increased size requires
the larger Aplanatic Ritchey-Chretien instrument to use dimmer stars to main-
tain the same probability of their occurrence within the field. For example,
assume that the effect on increasing the aperture D by a factor of ten
(N = 10) is being considered. Enter the curves at an aperture diameter = 1 D.
The field of view (the abscissa) can be read from the bottom curve as 1°.
The corresponding visual magnitude from the top curve is found to be 10
(M_V = 10). If the diameter is now scaled to 10 D, the field of view is re-
duced and the corresponding visual magnitude is read from the top curve as 13.

13

HENCE

$$\text{FOM} \triangleq \text{FIGURE OF MERIT} = \frac{E_{p\text{req'd}}}{E_{p_{min}}} \propto \frac{D}{\sqrt{2.51^{m_v} \Delta f}}$$

BECOMES

$$\text{FOM} \propto \frac{\sqrt{D}}{\sqrt{\Delta f}}$$

AND

$$\frac{\text{FOM}_{\text{large system}}}{\text{FOM}_{\text{small system}}} = \sqrt{N \frac{\Delta f_{\text{small system}}}{\Delta f_{\text{large system}}}}$$

Where N is the factor (>1)
by which the system
sizes differ

Figure 10. Figure of Merit (FOM) of a Large System
Compared to FOM of a Small System

The figure of merit for pointing performance can be modified to
include the guide star presence probability factor. The results indicate
that a large Aplanatic Ritchey-Chretien system can perform better than a
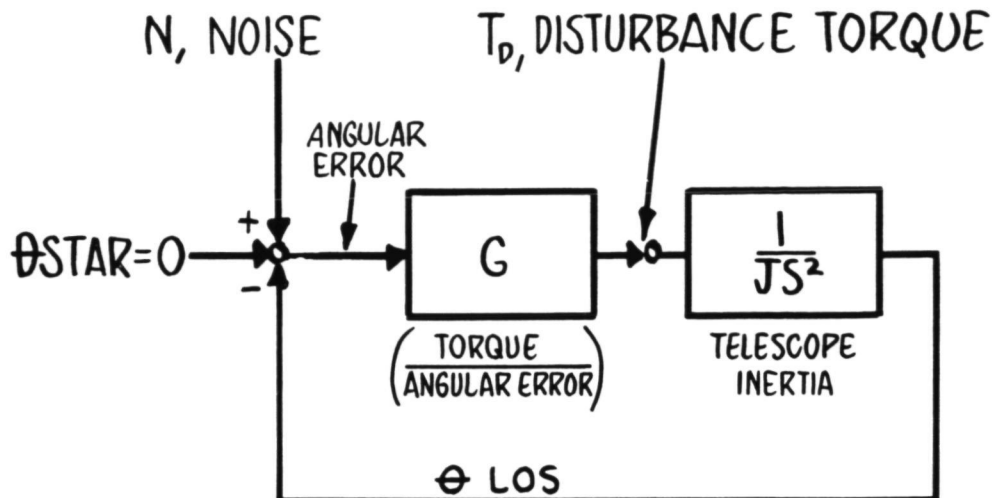small one if both have the same bandwidth.

$$FOM_{LS} = FOM_{SS} \sqrt{N \frac{\Delta f_{SS}}{\Delta f_{LS}} \left(\frac{1 + R_{SS}}{1 + \frac{R_{SS}}{N}} \right)}$$

WHERE R_{SS} IS THE BACKGROUND LIGHT PLUS DARK CURRENT EX-PRESSED AS SENSOR INPUT ENERGY DIVIDED BY THAT DUE TO SIGNAL ONLY---- FOR THE SMALL SYSTEM

AND N IS THE SIZE INCREASE FACTOR UNDER CONSIDER-ATION

Figure 11. Figure of Merit (FOM) of a Large System
Compared to FOM of a Small System

A more general expression for the Aplanatic Ritchey-Chretien two-mirror arrangement includes the effects of background light and phototube dark current. The derivation assumes that the phototubes and the size of the field stop (used ahead of the image splitter) are independent of system size.

N, NOISE T_D, DISTURBANCE TORQUE

ANGULAR
ERROR

$\theta STAR = 0$ +   —   G $\dfrac{1}{JS^2}$

$\left(\dfrac{TORQUE}{ANGULAR\ ERROR}\right)$ TELESCOPE INERTIA

θ LOS

$$\text{ANGULAR ERROR} = \frac{\dfrac{G}{JS^2}}{1 + \dfrac{G}{JS^2}}\, N(s) \approx N(s) \qquad ; \quad \frac{G}{JS^2} > 1$$

$$\approx \frac{G}{JS^2} N(s) \qquad ; \quad \frac{G}{JS^2} < 1$$

$$\text{ANGULAR ERROR} \quad \frac{\dfrac{G}{JS^2}}{1 + \dfrac{G}{JS^2}}\, T_D(s) \approx \frac{\left[\dfrac{T_D(s)}{JS^2}\right]}{\dfrac{G}{JS^2}} \qquad ; \quad \frac{G}{JS^2} > 1$$

$$\approx \frac{T_D(s)}{JS^2} \qquad ; \quad \frac{G}{JS^2} < 1$$

Figure 12.   Pointing Errors Dependence on Torque Disturbances

Torque disturbances produce additional pointing errors. While a smaller error due to noise results as servo bandwidth is reduced, torque induced errors increase.
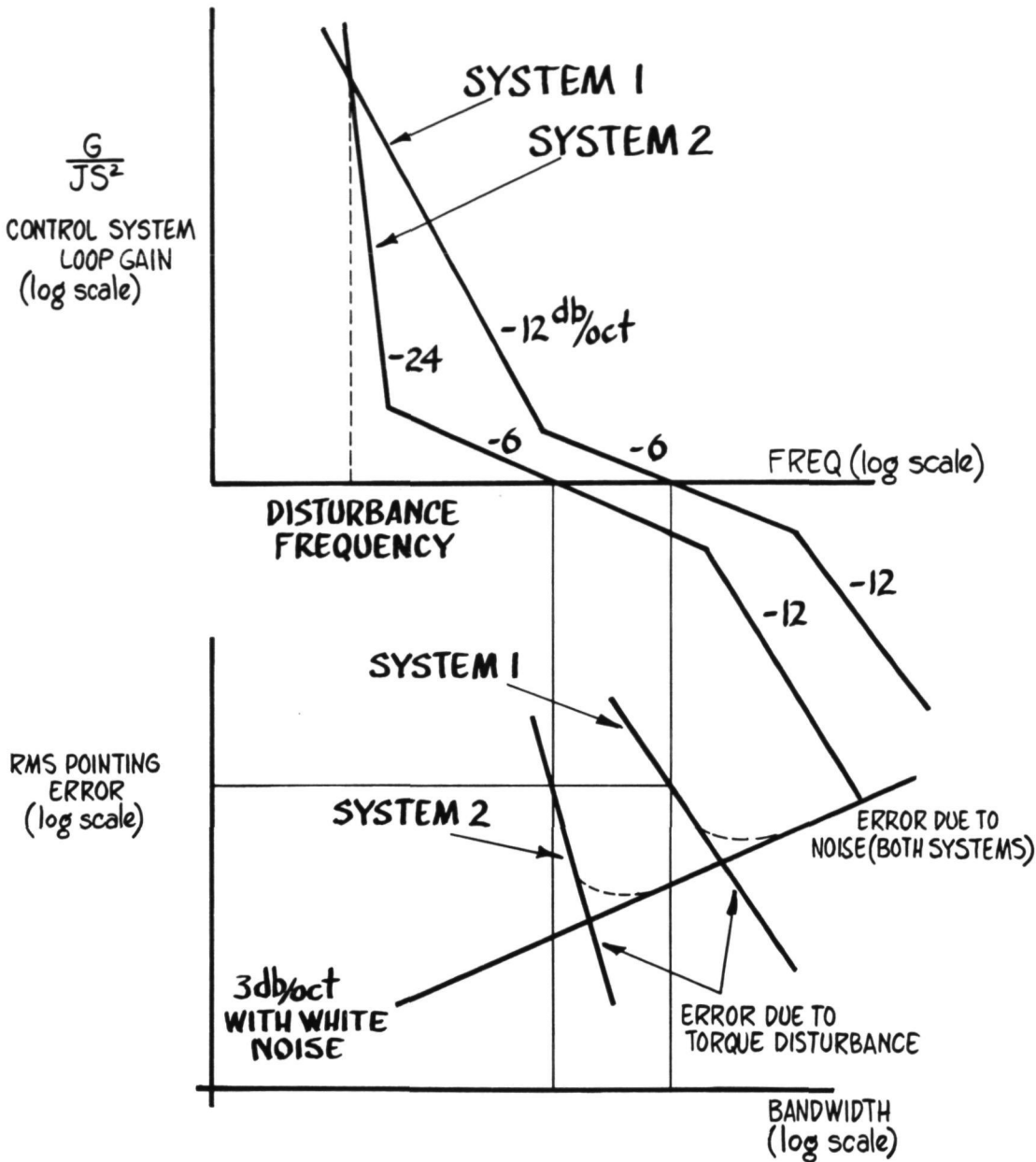
16

Figure 13. Pointing Servo Considerations for a Large
Space Telescope Experiment

Total errors can be reduced by selecting servo system character-
istics and bandwidth so that torque disturbance and noise produce comparable
pointing error components. For example, while both systems will have equal
errors due to torque disturbance, system 2 is superior since it has lower
bandwidth and therefore less error due to noise. Moreover, for the case
shown, a shift of the loop gain characteristic to the right will slightly
increase the bandwidth (and therefore the noise induced error), while rapid-
ly reducing the torque induced error. Minimum total error is obtained with
a bandwidth corresponding approximately to that at which the noise and
torque produced error curves intersect.

17

TYPICAL DISTURBANCE	SUSPENSION SYSTEM TYPE		
	FREE FLOATING	GIMBALLED	BODY POINT
• VEHICLE ORIGINATED: ASTRONAUT, MOMENTUM WHEELS, MISPOINTING	DECOUPLED	MINIMIZED BY GOOD BEARING ISOLATION AND OPTIMIZED VEHICLE-INSTRUMENT GEOMETRY	PRESENT
ENVIRONMENT ORIGINATED: SOLAR PRESSURE, GRAVITY GRADIENT	POSSIBLE	POSSIBLE	PRESENT
INSTRUMENT ORIGINATED: MOMENTUM WHEELS	PRESENT	PRESENT	—
ADVANTAGES	LEAST DISTURBANCES, VEHICLE POINTING UNCRITICAL	MORE EASILY GROUND TESTED	THERMAL CONTROL AND INTERCONNECTION PATHS MORE READILY IMPLEMENTED
DISADVANTAGES	GROUND TESTING MOST DIFFICULT	VEHICLE POINTING MORE CRITICAL	VEHICLE POINTING REQUIREMENTS ARE MAXIMUM

Figure 14.   Suspension System Experiment Considerations

Suspension systems chosen for a space optical system should provide greatest isolation from disturbance torques. While the free-floating approach appears optimum in this respect, ground testing may be impossible. The body point arrangement features rigid attachment of the telescope and vehicle and, thus, requires the highest pointing precision of the vehicle. This requirement can be avoided by including a transfer lens within the telescope to compensate for vehicle mispointing.
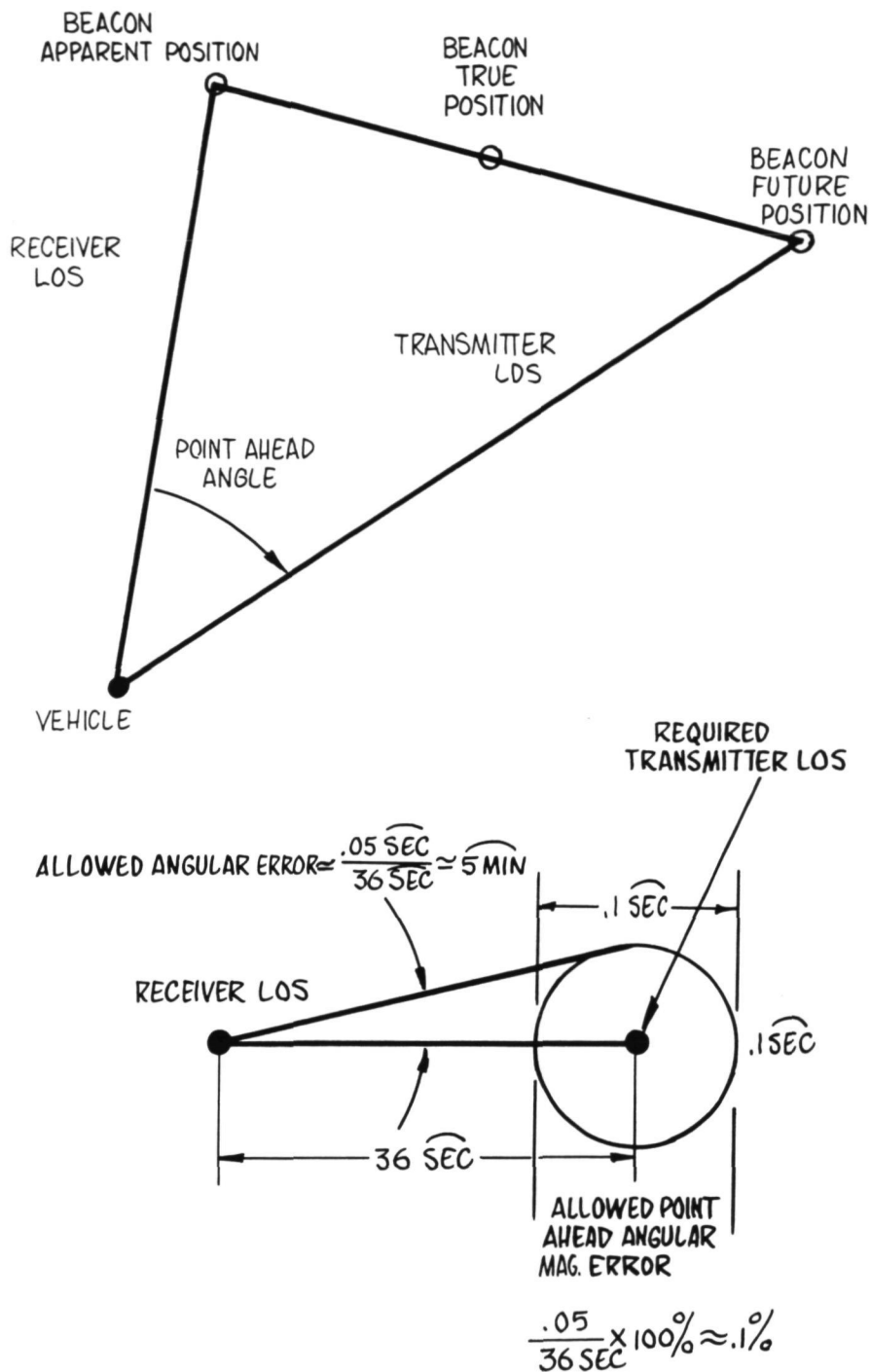
Figure 15. Point Ahead Experiment

Deep space point ahead magnitude and angle accuracy requirements are high, but they are considered within the state of the art. The information is slowly varying and can be transmitted to the vehicle over the ground beacon beam or over the microwave telemetry link.

POINT AHEAD COMMANDS
FROM COMPUTER

32" TELESCOPE WITH
POINT AHEAD CAPABILITY

20,000
MILES

$T_A = .7$
$\lambda = 6328 Å$
10 mw

.2 SEC

COMPUTER DERIVED
DIRECTIONAL COMMANDS

36 SEC DISPLACED
RECEIVER FOR POINT
AHEAD DEMONSTRATION

GROUND BEACON

≈ 3.2 MILES

DISTANCE REDUCED TO
NOMINAL ZERO VIA COMPUTER
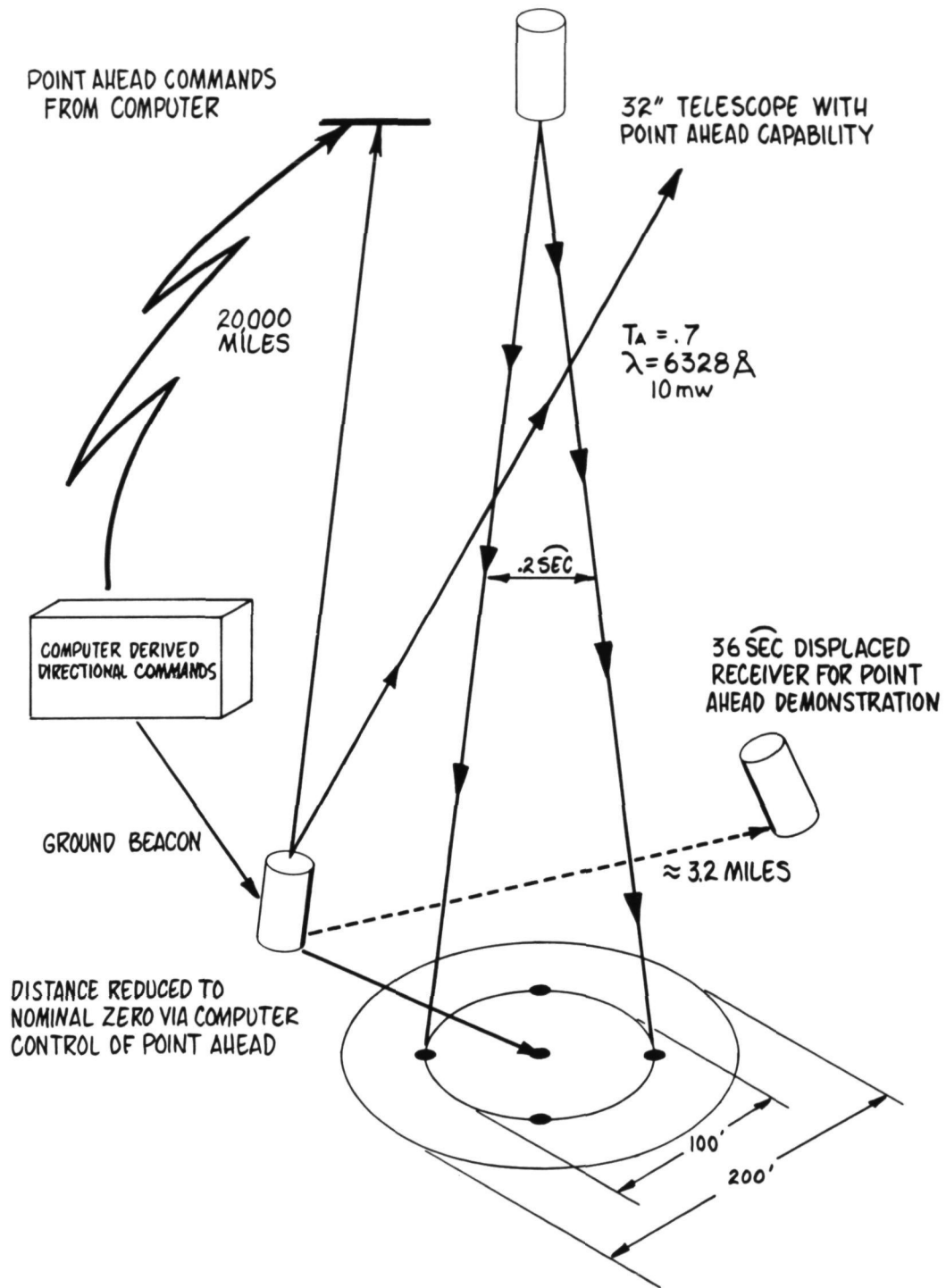CONTROL OF POINT AHEAD

100'

200'

Figure 16. Basic Equipment Arrangement for Pointing Experiments

In this typical configuration, a five-receiver array of intensity detectors on the ground monitors the position of the vehicle transmitted laser beam.

FIVE-RECEIVER ARRAY APERTURE
12" DIA. $^S/_N \geq 100$ FOV $\approx 1-4°$ (CRUDE
POINTING REQ'D) PREDECTION FILTERING 10A

50 FEET

UNCOOLED
DETECTOR
$I_D \approx 7 \times 10^{-14} w @ 6328 Å$

PREAMP
($\Delta f \approx 10 cps$)

SIGNALS TO COM-
PUTER FROM WHICH
POINTING ERROR
COMPUTED

10^{-8} watts
SIGNAL
(Temporally Coded)

SCINTILLATION COMPONENTS
EXPECTED---15% OF NOMIN-
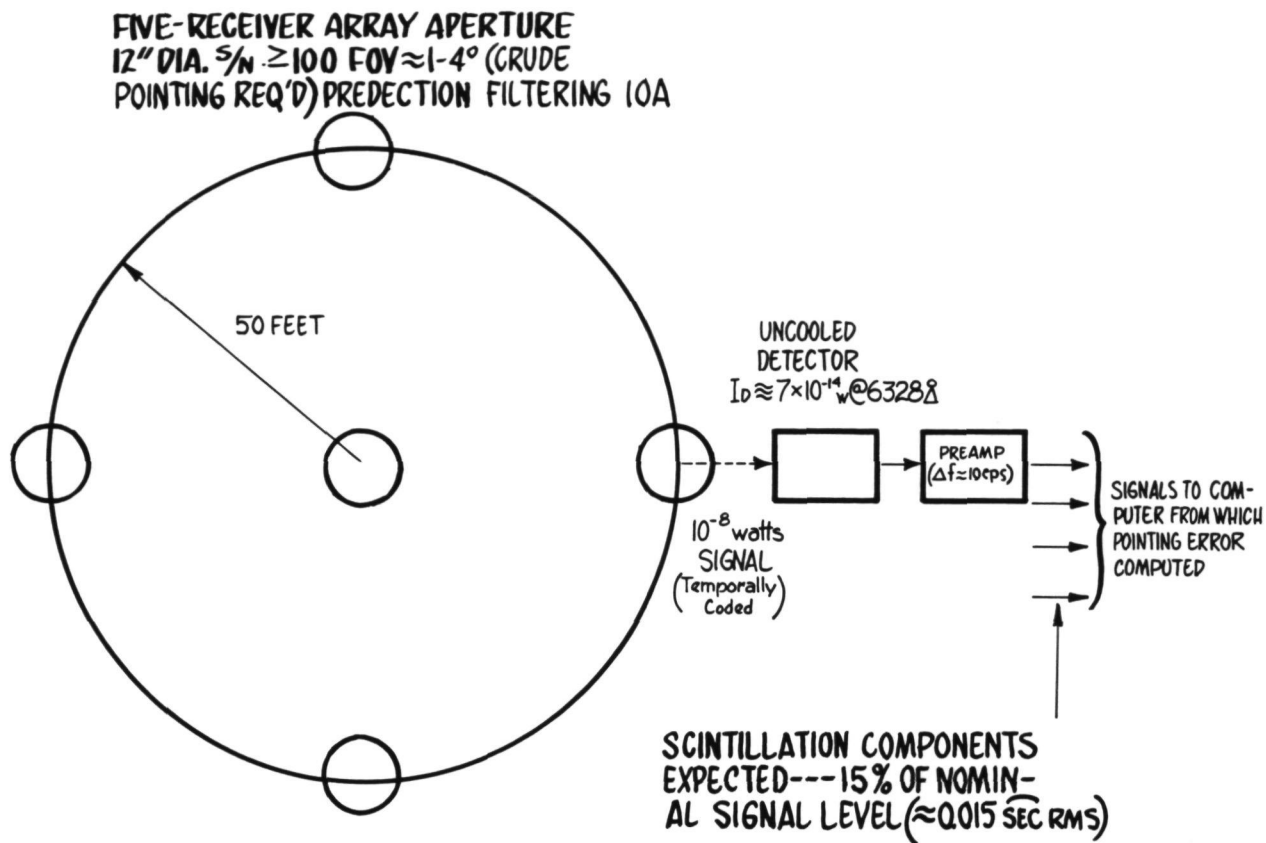AL SIGNAL LEVEL ($\approx 0.015 \widehat{SEC} RMS$)

Figure 17.   Some Parameters Associated with the Five-Receiver Array
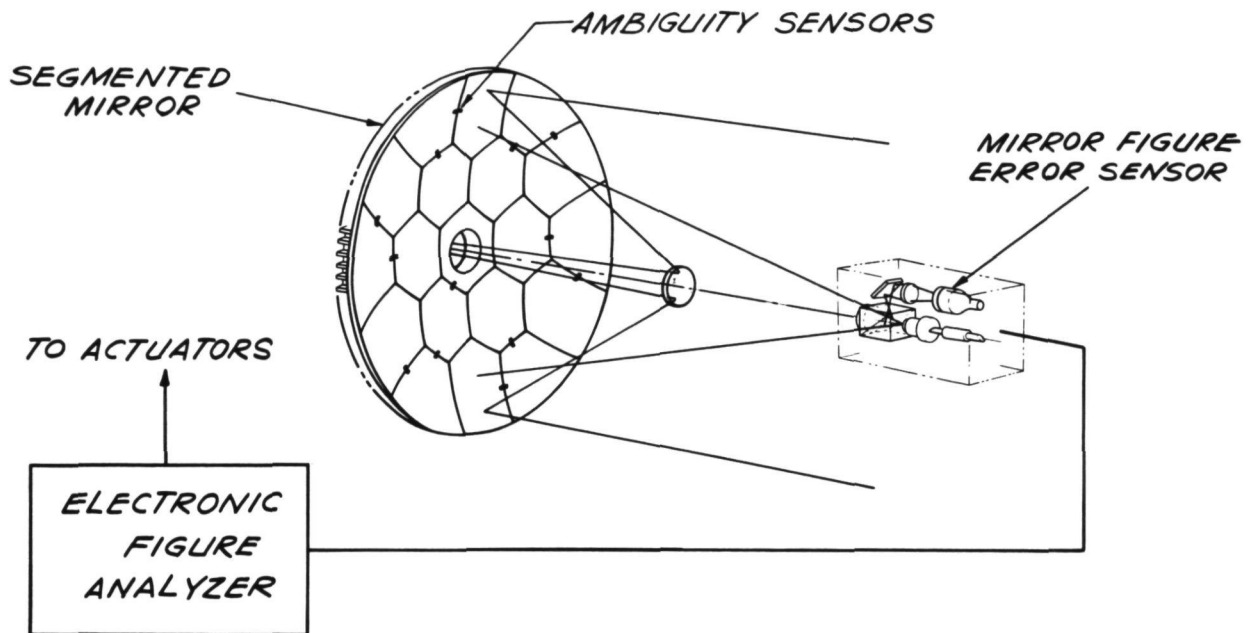of Ground Telescopes for Pointing Experiments

Figure 18. "Active Optics" Telescope System

The technique illustrated is the approach taken by Perkin-Elmer to the development of large diffraction-limited optical systems in space. Each of the individual hexagonal segments is positioned about 3 degrees of freedom by means of information obtained by the mirror figure error sensor located at the center of curvature. The ambiguity sensors are located near the primary mirror and are white-light interferometers. The experimental hardware of the phase measuring interferometer (fine figure sensor), the ambiguity sensors, and the mirror actuators are described in Figures 23 through 32.
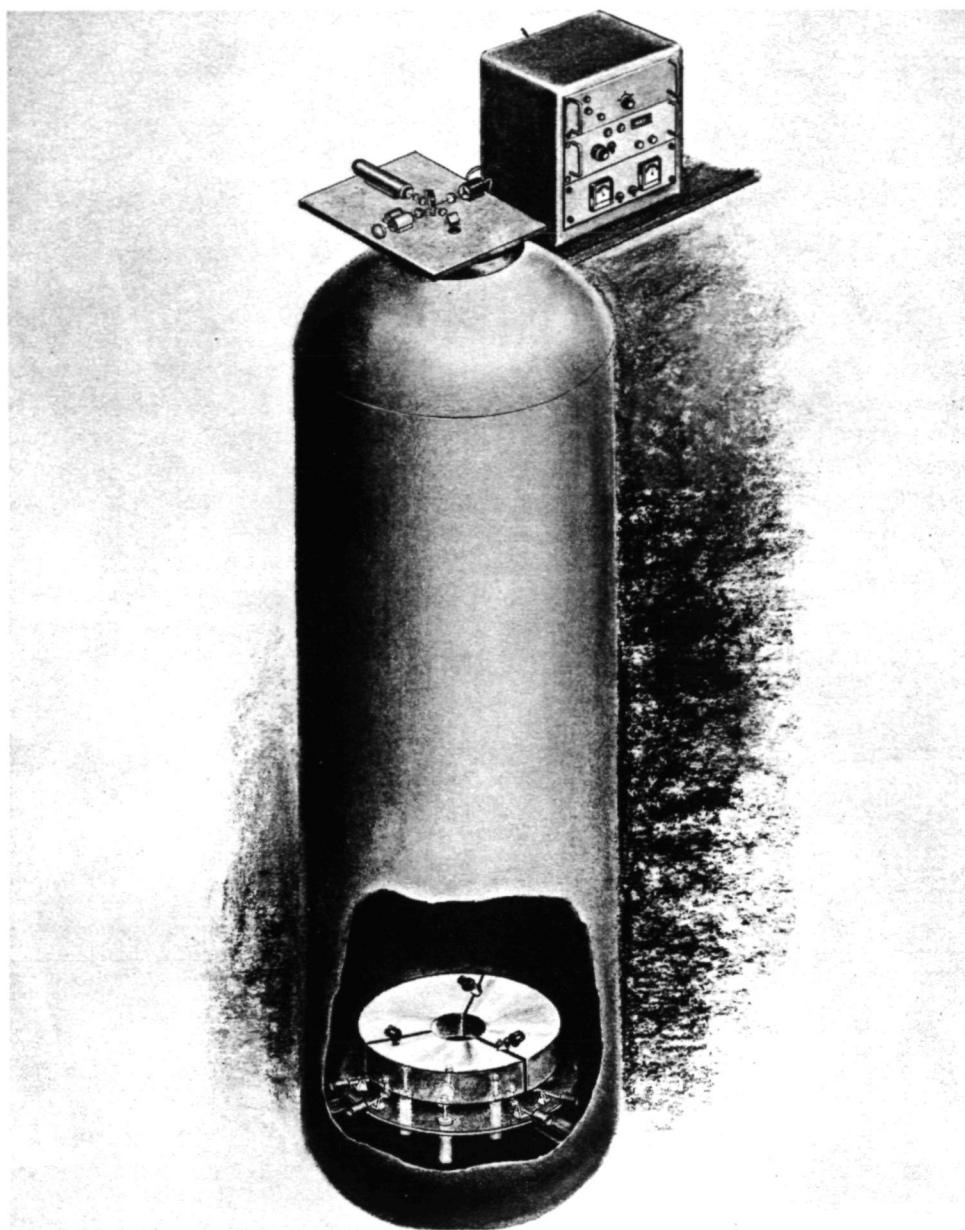
Figure 19.   Active Optics in Test Tank at Perkin-Elmer

This illustration shows the laboratory setup at Perkin-Elmer in
which a 20-inch solid fused quartz mirror is to be tested in the Vertical
Vacuum Tank Facility. The three segments will be moved into position by
three servo actuators for each segment in response to figure error commands
from the laser phase measuring interferometer located at the top of the
tank. Each segment is precisely counterweighted, as illustrated. White-
light interferometers are located between adjacent segments to position the
segments to $\lambda/4$. After coarse positioning by the white-light interferometers,
the fine figure sensor completes the positioning to $\lambda/50$ so that the overall
aperture achieves the performance of a continuous surface operating at its
diffraction limit.

CHANNEL SEPARATION
(OPTICAL DUPLEXING)

OBJECT: TO USE A COMMON TELESCOPE "FRONT END" FOR THE DUAL FUNCTIONS OF <u>RECEIVING</u> BEACON LIGHT IN DEEP SPACE AND <u>TRANSMITTING</u> INFORMATION BACK TO EARTH

BASIC OPTICAL CONFIGURATION: RECEIVING DETECTORS & TRANSMITTER LASER ARE PLACED AT CONJUGATE BACK FOCI
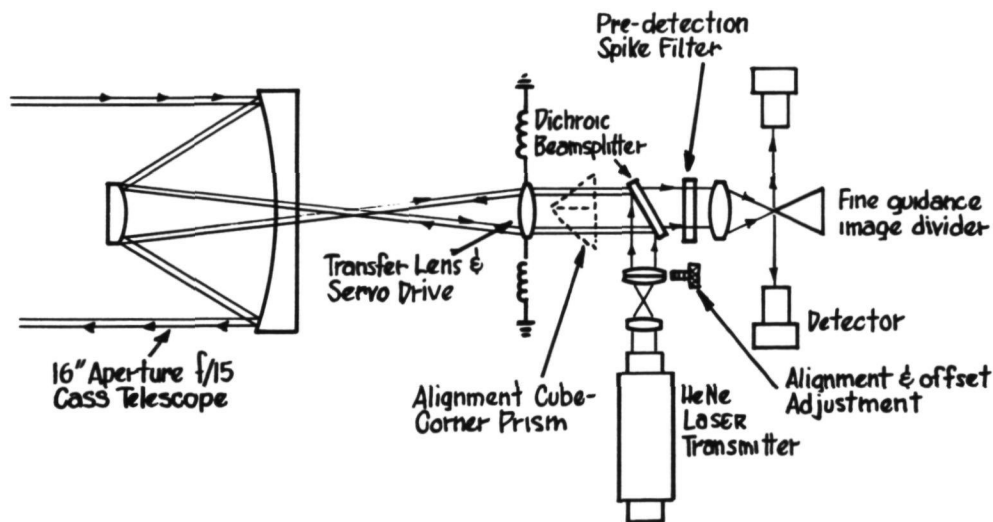

Figure 20. Channel Separation Investigation: Sources of Interference and Their Remedies

One hundred ten decibels of channel separation have been obtained to date (i.e., one part in 10^{11} of transmit laser light is detected in the fine guidance receive channel). The techniques developed can lead in principle to somewhat greater separation if necessary. The 110 decibel separation was obtained with a spaceworthy optical arrangement having a minimum of sensitive optical components.

SOURCES OF TRANSMITTER INTERFERENCE

A. LIGHT SCATTERED BY BEAMSPLITTER SUBSTRATE AND DIELECTRIC COATINGS

REMEDIES: 1."Control grind" substrates

2. Low-scatter coating techniques

B. LIGHT TRANSMITTED BY BEAMSPLITTER

REMEDIES : 1. Reduce transmission of beamsplitter to a minimum at 6328Å while maintaining maximum blue transmission

2. Provide efficient absorbers for transmitted component.

C. LIGHT REFLECTED FROM TRANSFER LENS

REMEDIES : 1. Apply very low reflective coatings

D. INCOMPLETE BLOCKING OF RESIDUAL RED LIGHT

REMEDIES : 1. Develop efficient spike filters with greatly enhanced suppression in the wings - particularly at 6328Å. Obtain suppression by incorporating new short-wave-pass-filter (SWPF) design into dielectric stack.

2. Use additional SWPF as needed.

3. Choose detector for maximum blue sensitivity and minimum red

Figure 21.   Scattered Light Sources with 6328Å Laser Transmitter

ALIGNMENT & POINT AHEAD

BY INSERTING A CUBE-CORNER PRISM INTO THE REGION SHOWN, AND BY ENSURING THAT THE DETECTORS HAVE BEEN MADE NO MORE INSENSITIVE TO RED THAN NECESSARY FOR ADEQUATE CHANNEL SEPARATION, ENOUGH 6328 Å LIGHT CAN BE MADE AVAILABLE TO DETECT EXACT REGISTRATION OF CON-JUGATE FOCI.

THIS IS THE BORESIGHT REFERENCE FROM WHICH POINT AHEAD IS INTRODUCED. OFFSET IS ACCOMPLISHED BY TRANSLATING LASER COLLIMATING LENS OR BY EQUIVA-LENT ROTATION OF RISLEY PRISMS

Figure 22.   Alignment and Point Ahead

The dielectric techniques for channel separation permit use of this simple technique for boresighting the transmit and receive channels.
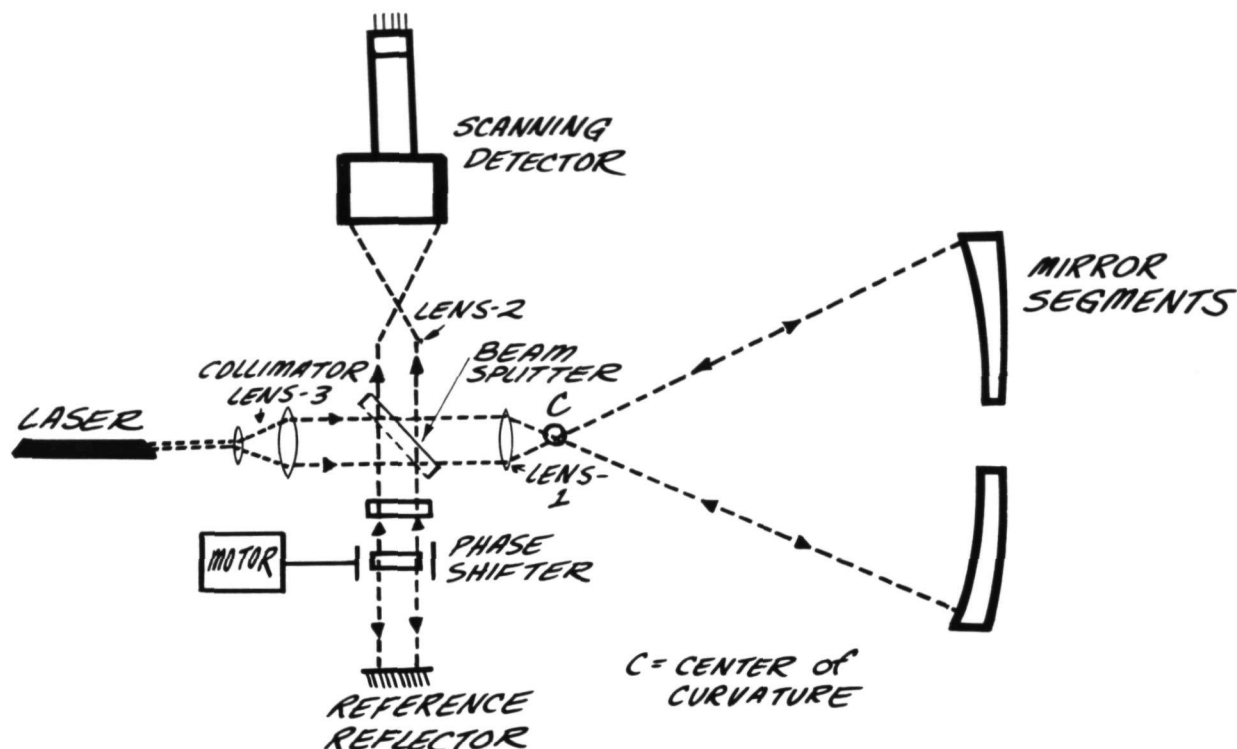
PHASE MEASURING INTERFEROMETER

Figure 23. Phase Measuring Interferometer

The equipment shown in this chart was demonstrated in the Perkin-Elmer Laboratory. The light from the laser is divided into two bundles by the beamsplitter. One bundle, transmitted by the beamsplitter, is converted to a spherical wave which, in turn, completely illuminates the spherical mirror. The reflected light from the spherical mirror is converted into plane waves with corrugations introduced by figure error, by the optical elements (Lens 1) and impinges on the beamsplitter. The light from the laser which was reflected by the beamsplitter is shifted in frequency by an optical phase shifter.

The light with the controlled phase delay is combined with the light reflected off the mirror at the beamsplitter. In the demonstration, the interference appeared as straight line fringes moving at a rate determined by the phase shifter rate due to intentional tilt of the mirror under test. If there are corrugations in the plane wavefront caused by a non-perfect mirror segment, the interference will be advanced or retarded in relation to other parts of the image due to the optical path difference. The scanning detector senses the changes in the interference pattern and, through associated electronics, converts the optical path length errors into actuator commands.

	LONG TERM DRIFT	*SHORT TERM FLUCTUATIONS* $T \approx 1 SEC.$
ELECTRONICS	*NEGLIGIBLE*	*NEGLIGIBLE*
INTERFEROMETER ONLY	$\approx 500\ DEG./HR.$	$\approx 1\ DEG.\ PEAK$
OVERALL, WITH MECHANICAL REF.	$450\ DEG./HR.$	$\sigma = 1\text{-}\frac{1}{3}\ DEG.$
OVERALL, WITH OPTICAL REF.	$5\ DEG./HR.$	$\sigma = \frac{1}{3}\ DEG.$

Figure 24. Figure Sensor Sensitivity

This chart summarizes the factors which contribute to the errors of the figure sensor and their short and long term variations. The second and third line items (Interferometer Only and Overall, with Mechanical Reference) are drift errors <u>absolute</u>; however, the figure sensor measures phase <u>difference</u>. Therefore, the last line (Overall, with Optical Reference) is the appropriate figure sensor stability number. In order to appreciate the stability of the device, the reader should recognize that for a plus, minus 1/60 wave measuring system, the corresponding phase shift is plus, minus 12 degrees.

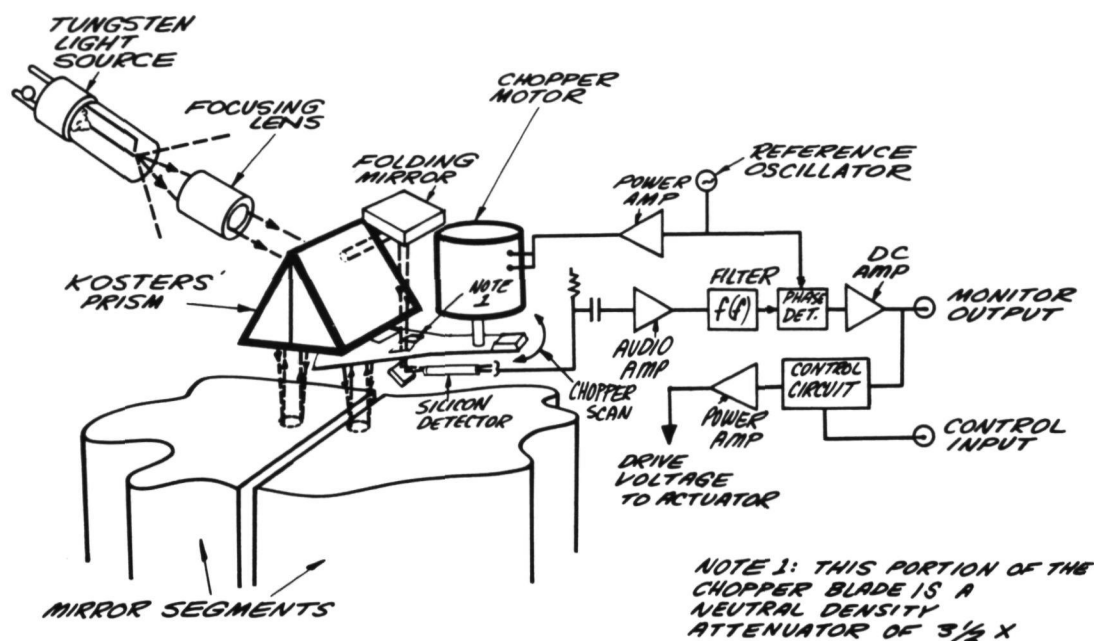# *WHITE-LIGHT INTERFEROMETER and POSITION SENSOR*

Figure 25. Ambiguity Sensor

Since the phase measuring interferometer can not differentiate between optical path lengths corresponding to a whole number of wavelengths, and since the mechanical structure locating the optical elements can not be made stable enough to position the mirror segments to less than one wavelength, a coarse alignment system is needed to position the segments to an accuracy of 1/4 wave. The white-light interferometer with its associated position sensor was demonstrated in the Perkin-Elmer Laboratory. This simple device utilizes a Kösters' prism to produce unambiguous white-light interference fringes. The demonstration used a small motor to drive one mirror segment into alignment with another mirror segment (4 microinches was the actual stop band used as shown in Figure 26).

COMPUTED INTERFEROGRAM
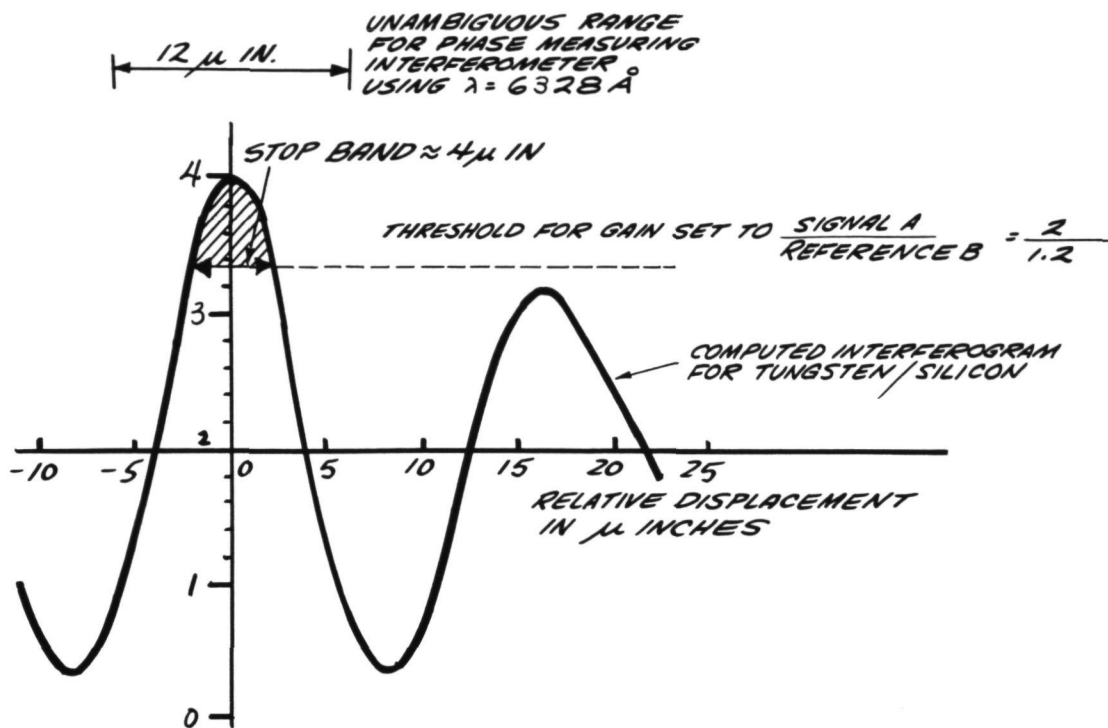
Figure 26. Coarse Alignment Requirements

This sketch illustrates where the 4-microinch stop band require-
ment for the white-light interferometer originates.

**POSITION SENSOR
CLOSED LOOP OPERATION**
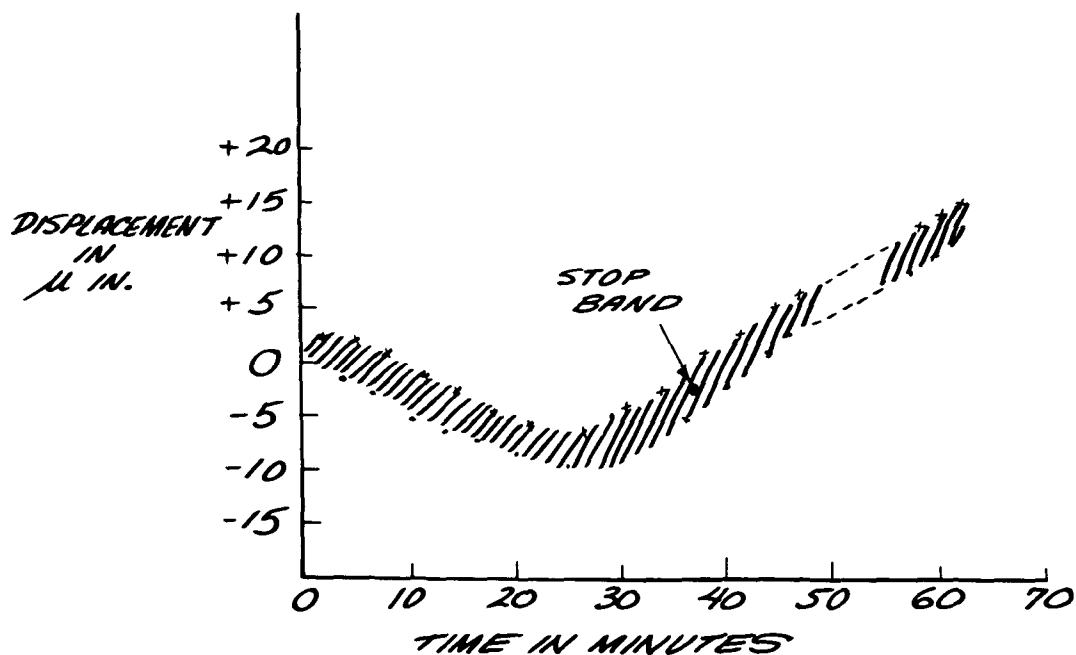
Figure 27. Measured Performance of the White-Light Interferometer

The stop band of the white-light interferometer (see Figure 26) for a number of measurements taken over a 60 minute period is shown in this chart. The width of the band indicates the uniformity of the positioning ability of the system. The curve of the band is due to thermal drifts in the setup.

31

SCAN PATTERN
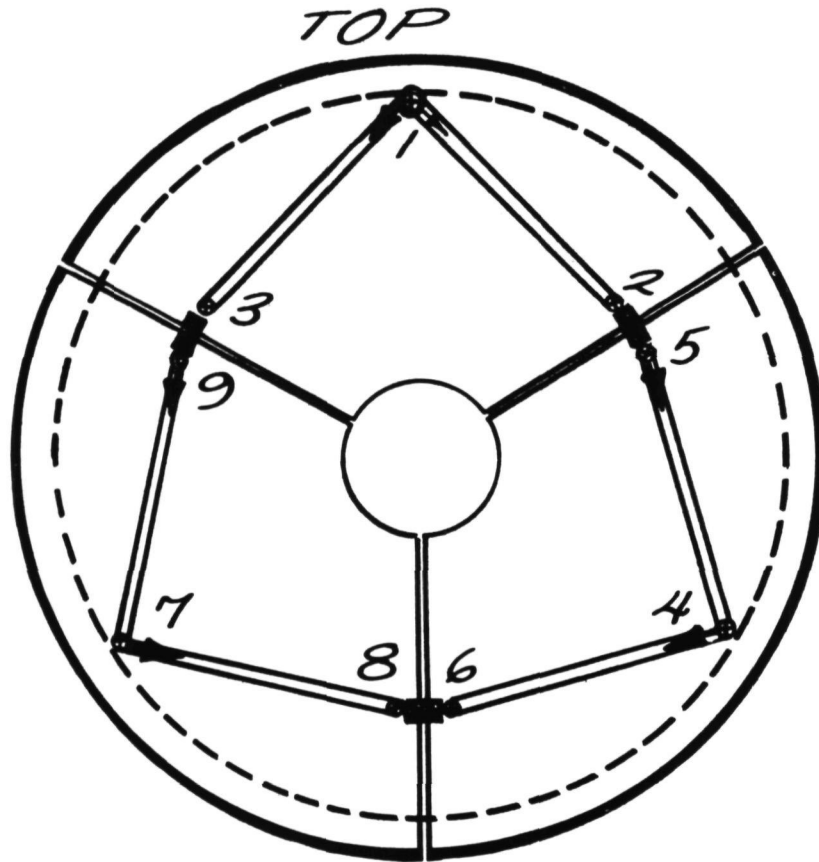
⊕ *ACTUATOR POSITIONS*

○→ *SENSOR SCAN*

⊕ *SENSOR REFERENCE POINT*

■■■ *KÖSTERS' PRISMS*

Figure 28. Arrangement of Actuators and White-Light Interferometers as Planned for the Laboratory Tests

ACTUATOR CHARACTERISTICS

1. SMALL DISPLACEMENTS
2. REVERSIBLE
3. LARGE DYNAMIC RANGE
4. LOW POWER CONSUMPTION
5. RELIABLE IN SPACE ENVIRONMENT
6. POSITIVE FORCE
7. FAST RESPONSE TIME

Figure 29. Desired Properties of Actuators for an Active Optics System

1. MAGNETOSTRICTIVE
2. ELECTROSTRICTIVE
3. MECHANICAL
4. THERMAL
5. ELECTROLYTIC
6. HYDRAULIC
7. PNEUMATIC
8. MAGNETIC
9. ELECTROSTATIC

Figure 30. Effects Which Might Be Used To Obtain
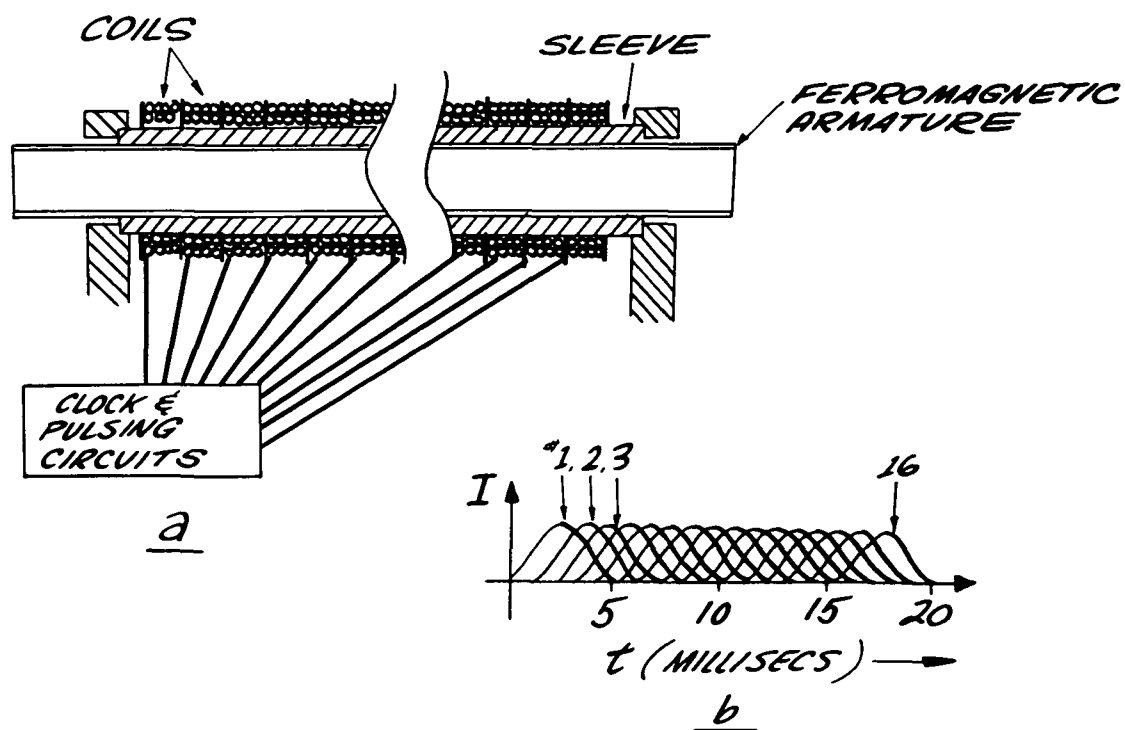Small Mechanical Displacements

Figure 31. Peristaltic Actuator

This device has been constructed and tested for use in the Active Optics Project. The armature advances as the magnetic field travels down the coils.
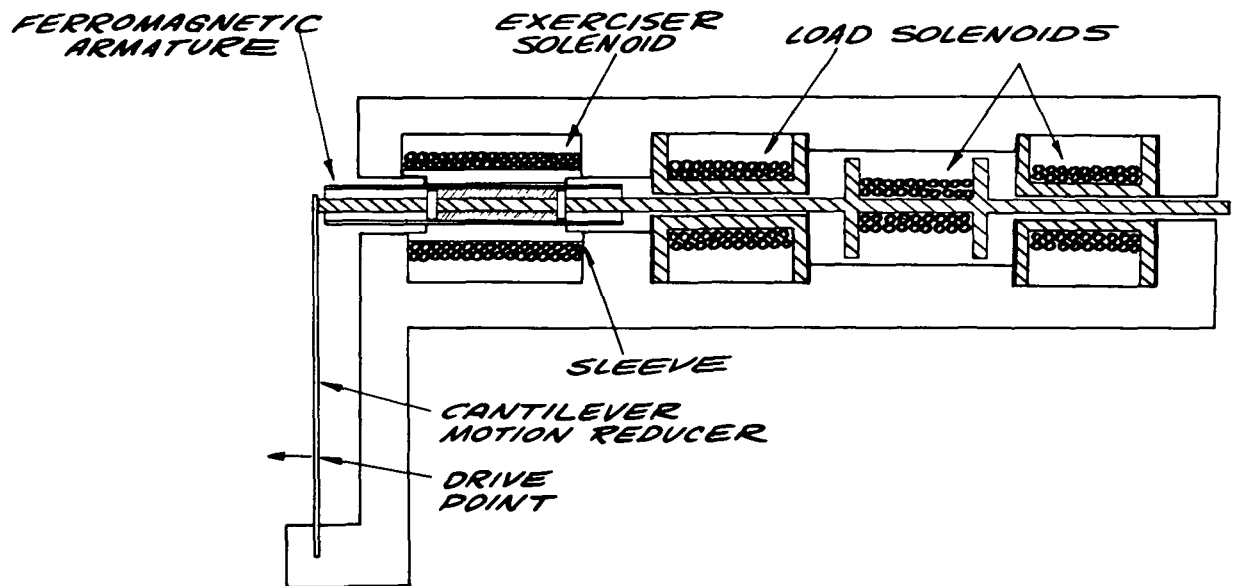
Figure 32. Magnetostrictive Load Actuator

This is the actuator that was demonstrated in the laboratory. Displacements of one microinch were demonstrated.

Candidate Space Optics Experiments/Demonstration	Test 1 Key Answers to Engineering Questions	Test 2 Must Experiment be in Space	Test 3 Important Scientific Activity	OTES Importance Rating Yes 10 / No 1	Applicability to Space Astronomical Instruments	Applicability to Space Laser Communications	Applicability to Reconnaissance	Applicability to Other Areas (Identified)	Cost to Conduct this Experiment on Independent Configuration (Not Otes)
*1 Mirror Figure Measurement on Earth Using Laser	Yes	Yes	Yes	9	Yes	Yes	Yes		
2 Remote Manual Optical Alignment		No		3	Yes	No			
3 Off Axis Telescope Performance					Yes	No	Yes		
4 Use of Astronaut to Effect Telescope Configuration Change	Yes	Yes	Yes		Yes	No			
*5 Verification of Telescope Pointing Precision Limits	Yes	Yes	Yes	9	Yes	Yes			
6 Thin Mirror	Yes		Yes		Yes	Yes	Yes		
7 Figuring Optical Surfaces in Space by Ionic Beams		Yes		1		No			
8 Mirror Coating Facility in Space	No	Yes	No	1	Yes	No	No		
9 Space and Radiation Effects on Optical Elements	No	Yes		3	Yes	Yes	Yes		
10 Radiation Noise Effects on Detectors in Pointing Loops	Yes	Yes	Yes	8	Yes	Yes	Yes		
11 Mirror Figure Measurements as a Function of Earthshine Input to Telescope	Yes	No	Yes	5	Yes	No	No		
12 Mirror Figure Measurements as a Function of Active Thermal Control	Yes				Yes				
13 Mirror Figure Measurements Correlated with Numerous Temperature Sensors	Yes				Yes	Yes			
14 Telescope Alignment Measurements Correlated with Numerous Temperature Sensors	Yes				Yes	Yes			
*15 3 Meter Segmented Active Optics Telescope	Yes	Yes	Yes	9	Yes		No		
16 Passively Cooled Telescope Structure, Mirror and Detector									
17 Occulting Disk Experiments		Yes			Yes	No	No		
18									
19 Utilization of Astronaut to Change Optical Segments	Yes	Yes	Yes		Yes	No	No		
20 Utilization of Astronaut to Measure Primary Figure with Scatter Plate Technique	No			3					
*21 Segmented Active Optics Techniques	Yes		Yes	9	Yes	No	No		
22 Thin Mirror Mechanical or Thermal Deformation Type of Active Optics	Yes	Yes	Yes	7	Yes	Yes	Yes		
23									
Candidate Space Laser Communication Experiments/Demonstration									
*24 Atmospheric Scintillation		Yes	Yes		No	Yes	No		
25 Atmospheric Polarization	No	Yes			No	No	No		
26 Heterodyning in Space		Yes	No	5			No		
*27 Heterodyning On Earth									
*28 1/10 Arc Second Tracking	Yes	Yes		9	No	Yes			
*29 Point Ahead	Yes	Yes		9	No	Yes			
*30 Space-to-Ground-to-Space Loop Closure	Yes	Yes	No	9		Yes			
*31 Tracking with Spacecraft Disturbances	Yes	Yes	Yes	9	Yes	Yes	Yes		
*32 Suspension System Comparisons	Yes	Yes		8		Yes			
33 Tracking Transfer between Ground Stations	Yes	Yes		9	No	Yes			
*34 Acquisition	Yes	Yes		9	No	No			
*35 Earthshine Effects on Acquisition and Track	Yes			6		Yes			
*36 RLOS	Yes	Yes		9	No	Yes			
*37 1-Megabit Laser Communication	Yes	Yes		9	No	Yes			
38 High Resolution Atmospheric Absorption Measurements	Yes	Yes	Yes	8	No	Yes			
Candidate Laser/Telescope Utilization Experiments									
39 U V and Visible Light Astronomy									
40 Planetary Reconnaissance									
41 Two Point Communication Link									
42 Satellite Inspection									
43 Weather Observer									
*44 Long Wave (IR) Astronomy									
45 IR Earth Sensing									

Figure 33. Candidate Experiments for OTES

This chart (Figure 33) indicates experiments which were under consideration for the Optical Technology Experiment System at the time of the January 18, 1966 meeting. Justification for candidate experiments is in process simultaneous with the search for other worthwhile experiments. The asterisk (*) preceding some of the candidate experiments indicates that the candidate was discussed in more detail during the meeting.
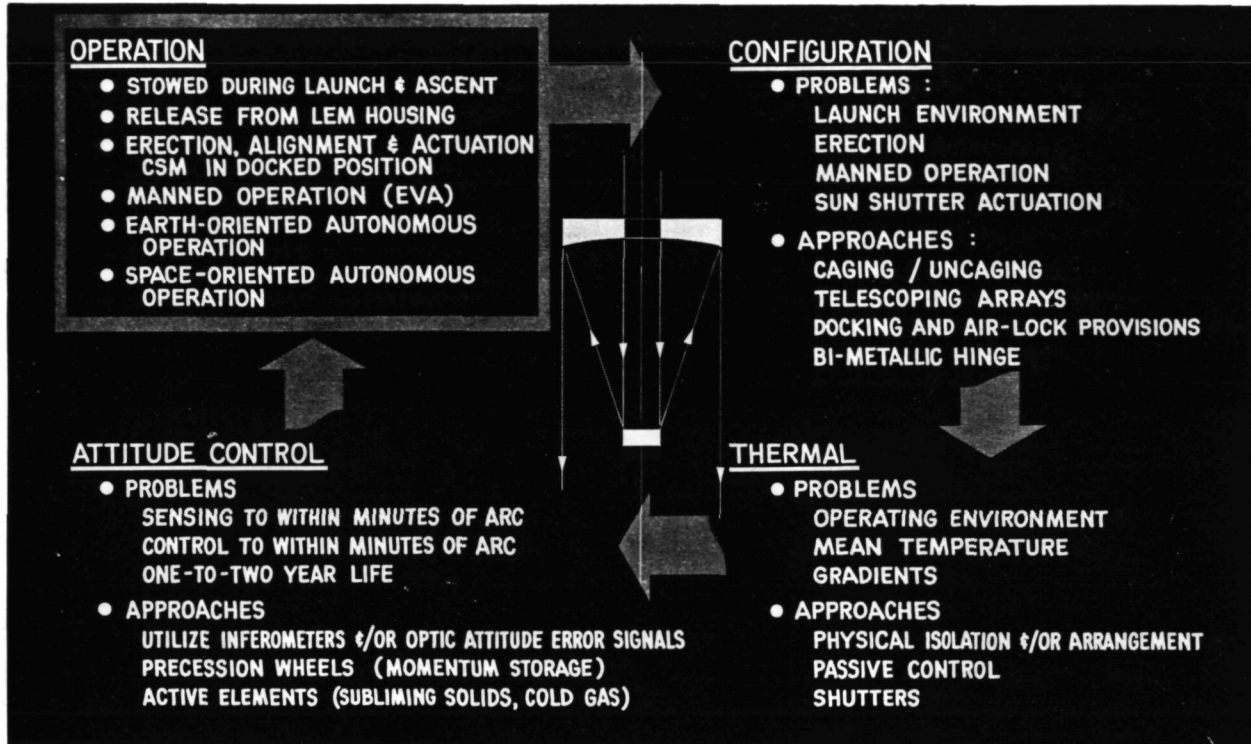
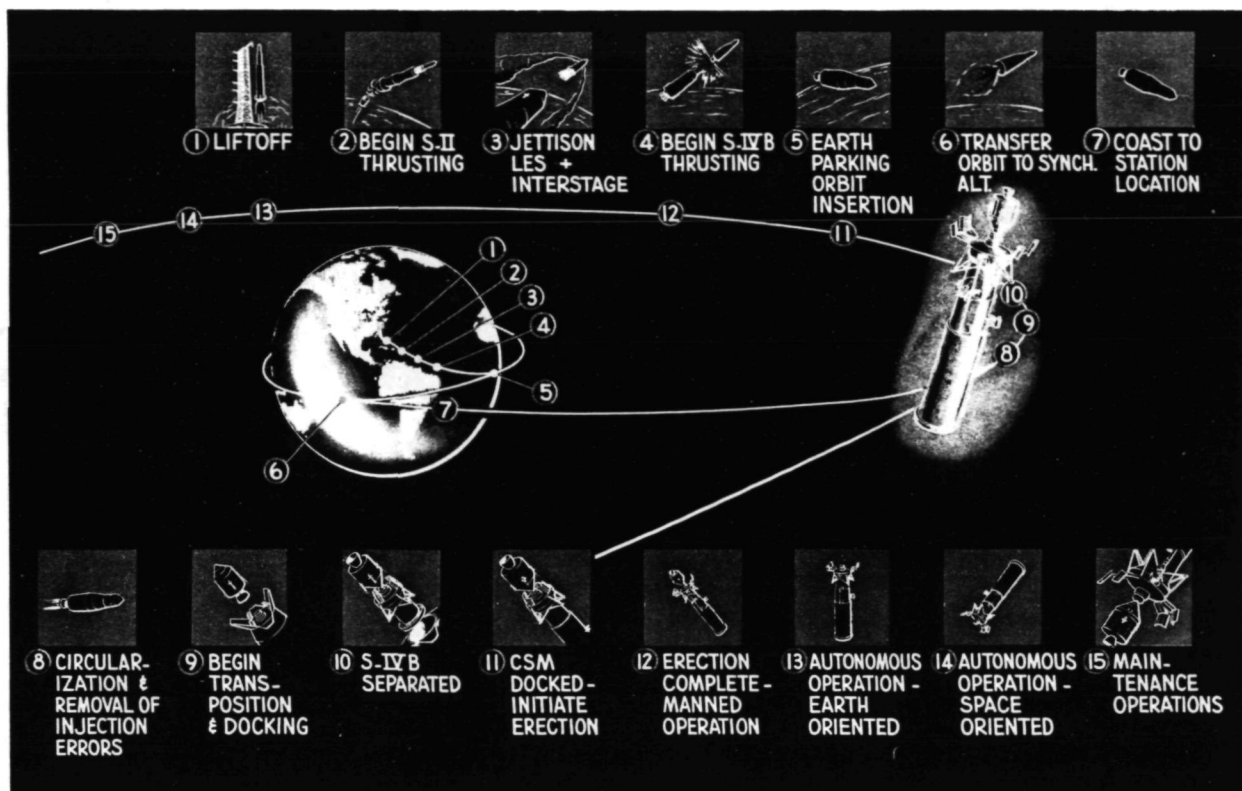Figure 34.   OTES Problem Areas Under Study by LMSC

Figure 35. Typical OTES Operational Sequence

The first ten steps illustrated in this operational sequence are typical of most Saturn V operations for a payload at synchronous altitude. Steps 11 through 15 are characteristic of the operations which would be needed to conduct the Three-Meter Aperture Experiment. In Step 11, the crew would dock the CSM to the telescope prior to the EVA operations necessary to assist the erection of the telescope from the stowed configuration (See Figure 36). Since the Three-Meter Telescope would restrict astronaut participation to 14 days, the initial group of experiments would be those experiments associated with manned operations (Step 12).

The astronauts would depart after 14 days, and the equipment would be required to perform the next group of experiments in the autonomous operation mode (Step 13). Although during Step 13 the telescope would point towards earth, Step 14 would comprise a group of experiments in which the telescope is pointed away from the earth. While in this mode, the 12-inch Laser Communicator Telescope is pointing toward the earth station transferring the scientific data back down to the earth station using the wide-band data channel. (See Communication Experiments #24 through 38 in Figure 33.) After several years of autonomous operation, a second CSM could rendezvous with the telescope as shown in Step 15 to perform routine maintenance and to up-date the equipment for new experiments.
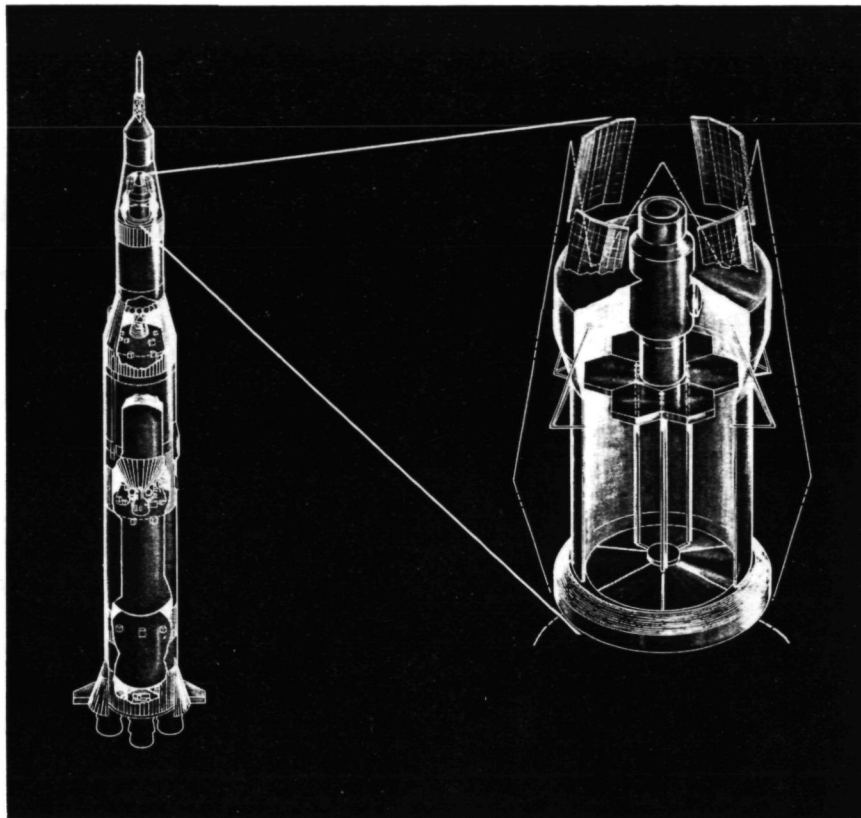
Figure 36.   The Three-Meter Concept in Boost Mode

In this sketch, the Three-Meter Telescope concept is housed in the available space inside the LEM Adapter with the solar panels and the sun shield folded. It is envisioned that auxiliary (secondary) experiments would be primarily housed within the service module pallet. The illustrated layout provides sufficient area for additional equipment and/or OTES payload growth. The system is stowed with the mirror segments assembled in their launch (or boost) structure.
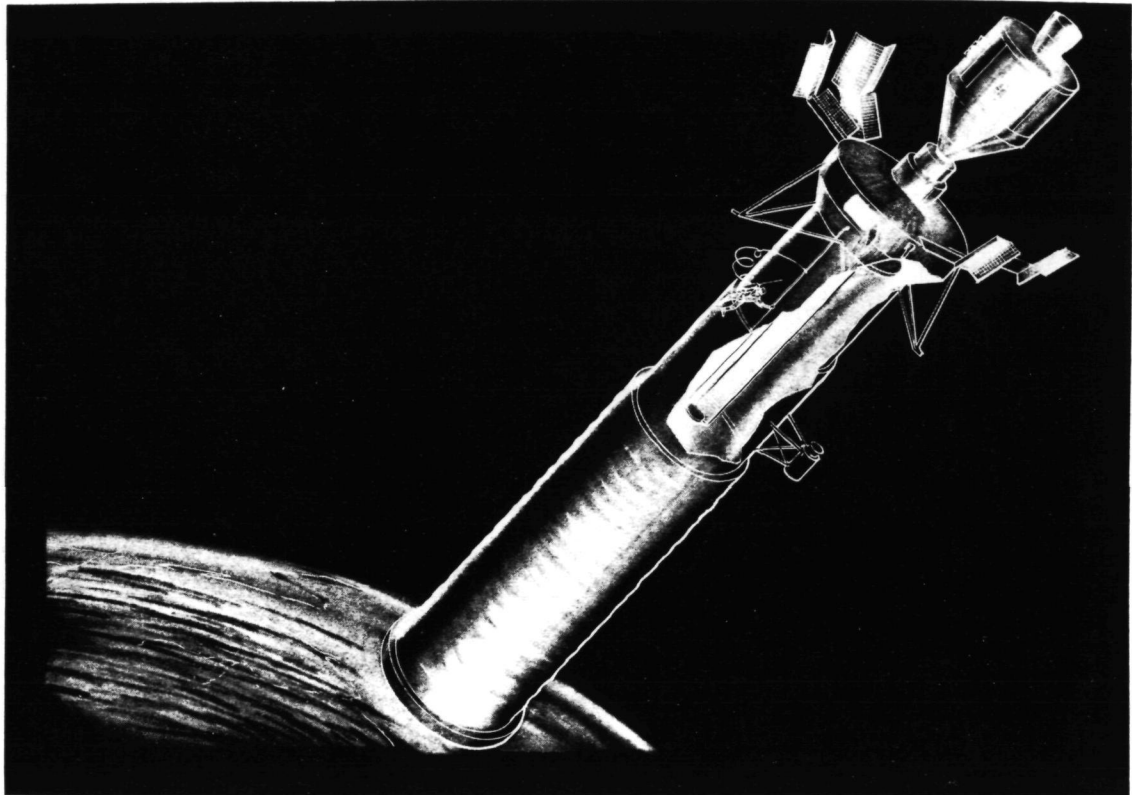
Figure 37. The Three-Meter Concept in Earth Oriented Mode

       This sketch indicates the postulated operational configuration. A minimum of steps are required to erect the OTES. These steps are (a) telescoping action of the telescope housing, (b) solar panel unfurling, (c) extension, rotation and locking of the three pair of quartz locating rods and (d) simultaneous unfurling of the sun shade and figure sensor/sun shutter equipment. An air lock behind the mirror facilitates astronaut operations.

- MEETS REQUIREMENTS/CAPABILITIES OF EXISTING AAP HARDWARE

- INHERENT SIMPLICITY ADAPTABLE TO HIGH RELIABILITY, LONG LIFE

- PROVIDES ALLOWANCE FOR AUXILIARY EXPERIMENTS (APPROX 7000 LB AND SERVICE MODULE PALLET AREA)

- INCLUDES AIR LOCK FOR INCREASED ASTRONAUT UTILIZATION AND SAFETY; REDUCED PRESSURIZATION REQUIREMENTS

- SIGNIFICANT DESIGN TOLERANCE FOR DESIGN IMPLEMENTATION PROBLEM RESOLUTION

- EASE OF MAINTENANCE/SERVICING. UTILIZE SAME DOCKING AND OPERATING TECHNIQUES AS ON INITIAL FLIGHT

- PROBABILITY FOR AN EXTENSION OF MISSION OPERATIONS

Figure 38. Principal Advantages of the Three-Meter
Concept (Figures 36 and 37)

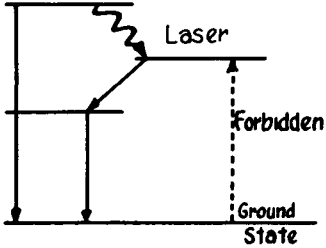| PLASMA	EMISSION WAVELENGTH	PRESENT POWER LEVELS	DATE FIRST REPORTED	AGE
He:Ne	6328Å	200 mW	June 1961	4½
A⁺	SEVERAL LINES ~5000Å	10 W	April 1964	2
CO₂:N₂:He	SEVERAL LINES ~10.6μ	150 W	June 1965	½

Figure 39. Gas Lasers of High Interest Today (1966)

CLASS I	CLASS II	CLASS III
PURE GASES & VAPORS e.g. Ion Lasers Ne (1.15) CO_2 Laser Forbidden Ground State Inversion by electron impact	GAS MIXTURES, DEPENDENT UPON COINCIDENTAL ENERGY LEVEL MATCH. (within kt) e.g. He-Ne Cs-He (optical pump) CO_2-N_2	GAS MIXTURES, NO EXACT ENERGY MATCH REQUIRED. PHYSICAL PROPERTY OF ADDITIVE IMPORTANT OR DISSOCIATION BY METASTABLE. e.g. O_2-A CO_2-He

Figure 40. Gas Laser Classes

PARAMETER	He:Ne	A⁺	CO₂
OUTPUT POWER	MODERATE($\frac{1}{4}$W)	HIGH(10W)	VERY HIGH [POSSIBLY 1KW]
EFFICIENCY (well above threshold)	POOR(10^{-4}-10^{-3})	POOR(10^{-4}-10^{-3})	VERY GOOD (10^{-1})
DETECTABILITY	GOOD	VERY GOOD	GOOD *(FOR COHERENT DETECTION)
RELIABILITY(with maintenance)	GOOD	POOR	GOOD
RELIABILITY(remote)	GOOD	POOR	(POOR)
SIZE	MODERATE	LARGE	LARGE
LIFE	LONG(>5000h)	SHORT(~200h)	LONG
COST	MODERATE	HIGH	LOW
BIGGEST PROBLEM	LIMITED POWER	CONTAINMENT OF PLASMA	FLOWING GAS

Figure 41. 1966 Gas Laser Comparisons

PREDICTIONS FOR GAS DISCHARGE LASERS

1. THERE WILL NOT BE A LASER OPERATING IN THE VISIBLE WITH THE EFFICIENCY OF THE PRESENT CO_2 LASER

2. ANY LASER GIVING WATTS OF VISIBLE RADIATION CAN BE EXPECTED TO HAVE THE SAME PROBLEMS AND POOR EFF-ICIENCY OF AN ARGON LASER

3. FUTURE EFFICIENT (>10%) HIGH POWER LASERS WILL PROBABLY HAVE A WAVELENGTH GREATER THAN 5 MICRONS
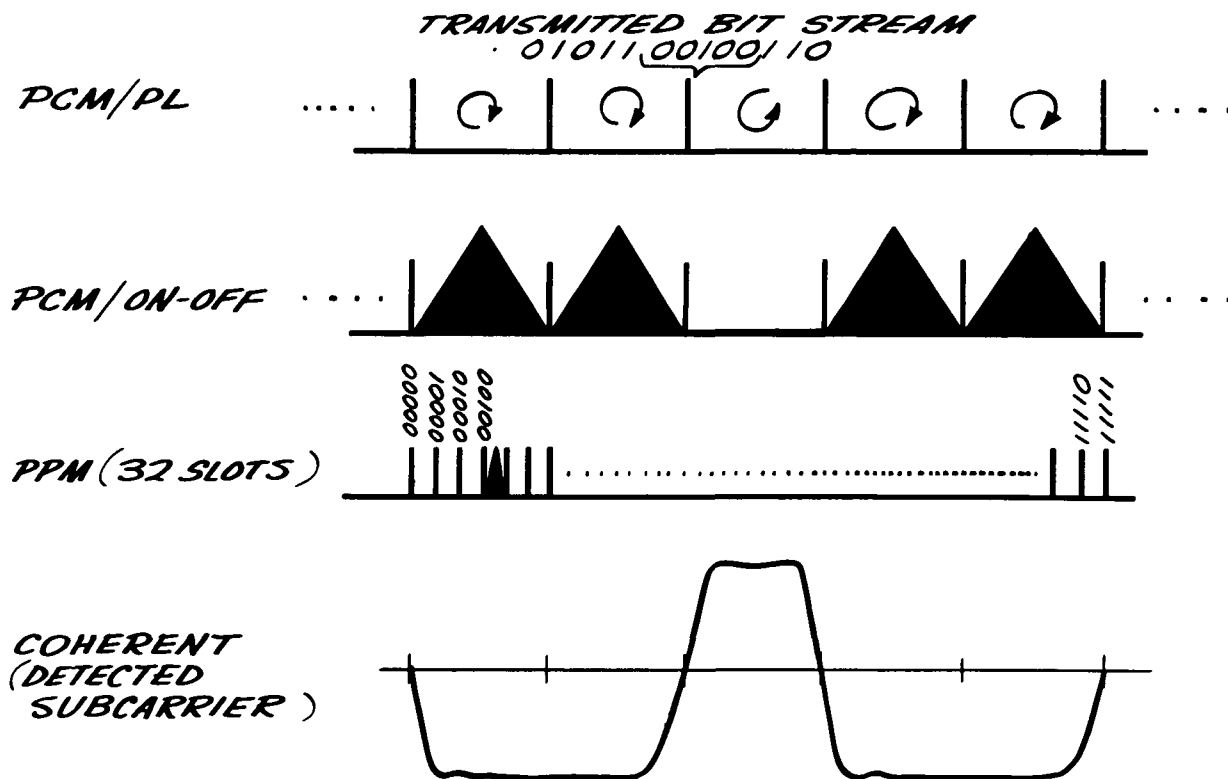
Figure 42.   Gas Lasers in the Future

Figure 43. Modulation Techniques

This figure demonstrates the method used to encode five bits of information on an optical signal.

DOWNWARD TRANSMISSION λ	INTENSITY DETECTION		COHERENT DETECTION
	.6328 μ	1.0 μ	10.6 μ
RANGE - STAT. MILES	10^8 ———————		→
TRANSMITTER APERTURE (METERS)	1	1.2	1.5
BEAM DIVERGENCE (μ RADIANS)	.63	.83	7.07
EFFECTIVE RECEIVER APERTURE (METERS)	10	10	4
RECEIVER FIELD of VIEW (SEC)	20	20	
ATMOSPHERIC TRANSMISSION (q=60°)	.70	.9	.30
OPTICAL SYSTEM TRANSMISSION	.50	.50	.50
PRE DETECTION FILTER	.15 → .5 Å .80 → 5 Å	.60 → 50 Å .65 → 100 Å	.60 → .08 μ .80 → .15 μ .90 → .3 μ
"BLUE" SKY $\frac{watts}{m^2-ster-\mu}$	5×10^{-7}	5×10^{-8}	3.4×10^{-8}
DETECTOR	RCA 7265	RCA 7102	Ge:Hg
AT TEMPERATURE	-70°C	-70°C	30°K
DARK CURRENT (WATTS)	2×10^{-15}	10^{-14}	
$D^* \frac{m (cps)^{1/2}}{watt}$			10^9
QUANTUM EFFICIENCY	.05	.001	.20
DOPPLER (MAXIMUM)	.35 Å	.57 Å	1.7 kMcps
DOPPLER RATE (MAXIMUM)	5×10^{-7} Å/SEC	10^{-6} Å/SEC	3.5 kcps/sec
SIGNAL PHOTOELECTRONS RECEIVED FOR EACH WATT TRANSMITTED	1.3×10^8	8.8×10^5	8.1×10^6
OPTICAL FILTER	.5 Å	50 Å	.3 μ
BACKGROUND & PMT NOISE PHOTOELECTRONS / SEC.	1.75×10^{17}	3.7×10^7	

Figure 44. Helium-Neon, YAG, and CO_2 Communication
System Comparisons

This figure lists the constants assumed in the computation of
the receiver signal and noise powers measured at the output of the photo-
detectors.

TABLE II - BIT ERROR RATE = 10^{-3}

MODEM	DATA RATE = 10^6 bps					DATA RATE = 10^4 bps				
	PCM/PL	PCM/ON-OFF	PPM 32 Slots	PPM 512 Slots	COHERENT	PCM/PL	PCM/ON-OFF	PPM 32 Slots	PPM 512 Slots	COHERENT
WAVELENGTH (μ)	.6328	.6328	1.	1.	10.6	.6328	.6328	1.	1.	10.6
SAMPLING INTERVAL (T) (SECONDS)	10^{-6}	10^{-6}	3×10^{-8}	2×10^{-9}	10^{-6}	10^{-4}	10^{-4}	3×10^{-6}	2×10^{-7}	10^{-4}
NOISE COUNT PER T (PHOTOELECTRONS)	13	13	1.1	.075		1300	1300	110	7.4	
SIGNAL COUNT PER T (PHOTOELECTRONS)	18	30	13	8		300	500	60	24	
REQUIRED TRANSMITTER POWER (watts) OP	.14	.23	3.	1.	20.	.023	.040	.13	.03	.2
REQUIRED TRANSMITTER POWER (watts) EL	140	460	-	-	200	23	80			20

Figure 45.   Laser Communication System Performance Comparison

The required optical (OP) and electrical (EL) transmitter power is computed assuming that the He-Ne laser is used for PCM/PL, PCM/on-off, the Q-switched sun pumped YAG for PPM, and the CO_2 laser for coherent reception.
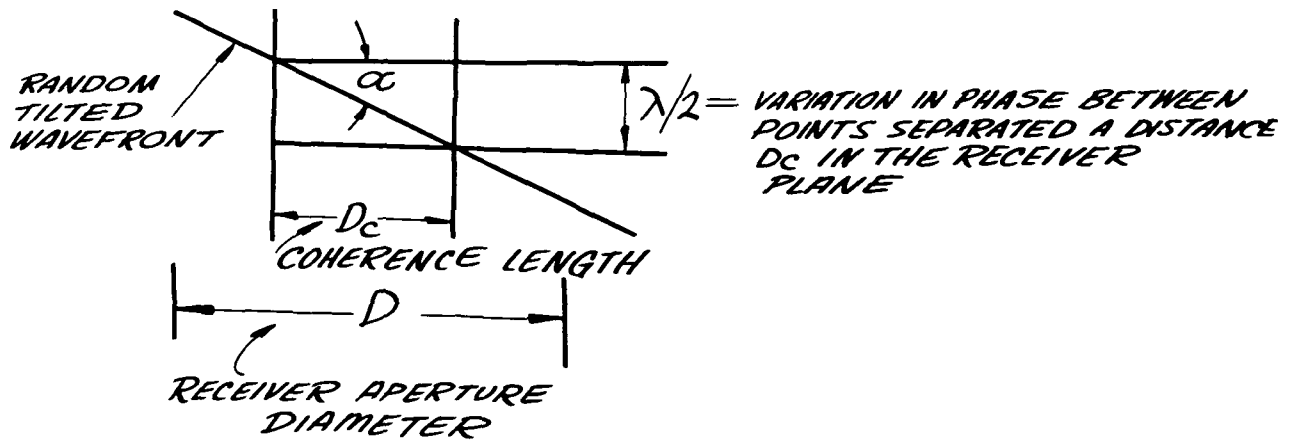
IDEALIZED WAVEFRONT

OPTICAL HETERODYNE ON EARTH

Figure 46. Dependence of Coherence Length Upon
Wavefront Tilt and Wavelength

Estimating the lateral coherence diameter on earth and its wave-
length dependence requires consideration of the wavefront distortion caused
by atmospheric turbulence. The simplest form of distortion is a random tilt-
ing of the signal wavefront. This figure shows the geometry of a wavefront
tilted by an angle α.

ANGULAR RESOLUTION LIMITED BY ATMOSPHERE: $\theta_A = \lambda/D_c$

COHERENCE DIAMETER: $D_c = \lambda/2\alpha$

$$\theta_A = 2\alpha$$

FOR IDEALIZED WAVEFRONT, IMAGE BLUR IS DIRECTLY RELATED TO WAVEFRONT DISTORTION INDEPENDENTLY of WAVELENGTH

$$\therefore \ D_c^2 = \lambda^2/\theta_A^2$$

ALL OTHER FACTORS EQUAL, OPTICAL HETERODYNE EFFICIENCY _IMPROVES_ WITH _LONGER WAVELENGTHS_ AND IS DEGRADED by _ATMOSPHERIC SEEING LIMITATIONS_

Figure 47. Optical Heterodyne Detection

This figure shows the mathematical relationships between image blurring, wavefront distortion, and coherence diameter for the simplest form of wavefront distortion.
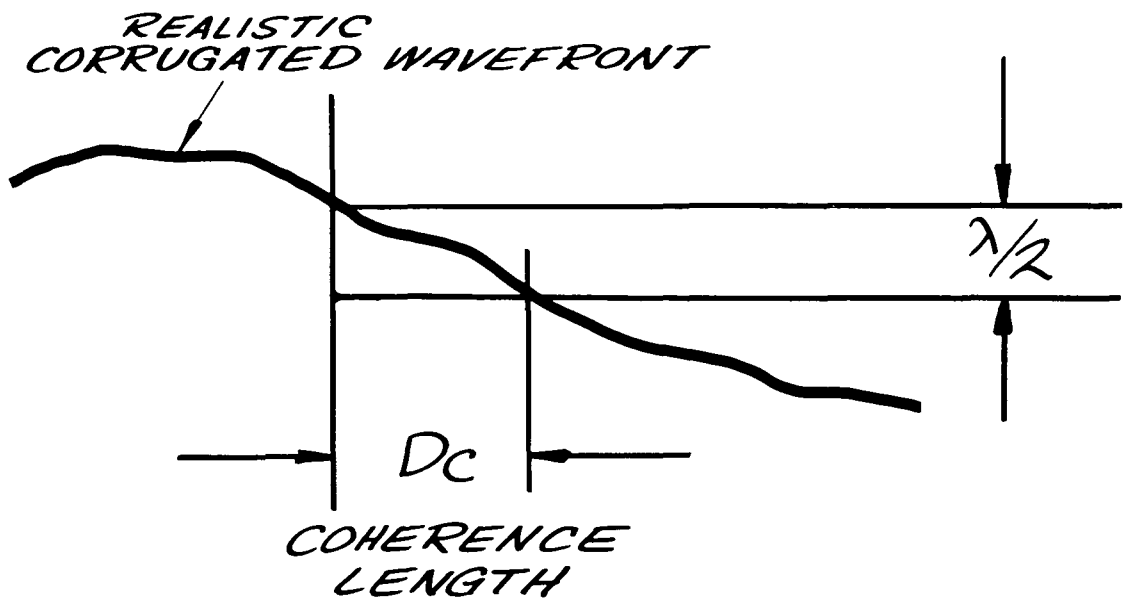
Figure 48.   Dependence of Coherence Length Upon
Wavefront Tilt and Wavelength

A realistic wavefront distortion is depicted showing the random
deviation of the wavefront about an average value.

$$D_C \sim \lambda^{1+\varepsilon}$$

$$\varepsilon = SMALL\ POSITIVE\ NUMBER \approx 1/5$$

$$\therefore D_C \sim \lambda^{6/5}$$

$$\therefore \theta_A \sim \lambda^{-1/5}$$

$$\lambda = 0.5\mu,\quad \theta_A \sim 1\ ARC\text{-}SECOND,\quad D_C \approx 10\ cm.$$

$$\lambda = 10\mu,\quad \theta_A \sim 0.5\ ARC\text{-}SECOND,\quad D_C \approx 4\ m.$$

Figure 49.   Optical Heterodyne Detection for
Realistic Wavefront Deformation

For the case of more realistic wavefront distortions, there is a
tendency of the wavefront to return to its average value. This figure shows
the relationships between coherence diameter, atmospheric limited angular
resolution, and wavelength. At half micron wavelength, the atmospheric lim-
ited resolution is typically 1 arc second for nighttime operation at sites
that would normally have good seeing. The corresponding lateral coherence
diameter is approximately 10 cm. For 10μ operation the image blur is approx-
imately 0.5 arc second with a corresponding lateral coherence diameter of 4
meters.

EXPERIMENT OBJECTIVES:

MEASUREMENT of FLUCTUATION of LIGHT INTENSITY from a COHERENT SOURCE AFTER PASSAGE THRU ENTIRE ATMOSPHERE

    (A) EARTH-TO-SPACE CRAFT
    (B) SPACE CRAFT-TO-EARTH

VARIOUS RECEIVER APERTURE SIZES
AT LEAST TWO LASER WAVELENGTHS
DAY & NIGHT OPERATION
SEVERAL ZENITH ANGLES
VARIOUS METEOROLOGICAL CONDITIONS

OPTICAL COMMUNICATION TECHNOLOGY BENEFITS

1. DETERMINATION of SUSCEPTIBILITY of COMMUNICATION SYSTEM To FADING

2. DETERMINATION of NOISE LEVELS & DYNAMIC REFRACTION EFFECTS

TECHNOLOGICAL BENEFITS:

1. ALLOWS MEASUREMENTS of ATMOSPHERIC SCINTILLATION from SPACECRAFT TO EARTH ON A COHERENT SOURCE

2. ALLOWS COMPARISON of EARTH BASED MEASUREMENTS of STELLAR SCINTILLATION WITH LASER BEACON MEASUREMENTS

Figure 50. Atmospheric Scintillation and Image
Jitter Experiments

      This figure depicts the experimental objectives, optical communication benefits, and other technological benefits of the atmospheric scintillation and image jitter experiments for the OTES Program.

SPACE CRAFT TRANSMITTER DATA

OPTICAL : He-Ne .6328μ } WITH LOW FREQUENCY
He-Ne 1.15μ } MODULATED TRACKING
SIGNATURE

MICROWAVE TELEMETRY : LASER POWER LEVEL MONITOR

EARTH RECEIVER DATA :

OPTICAL : DETECTION OF LASER BEACON INTENSITY
FLUCTUATION

ELECTRICAL : LOW AND HIGH FREQUENCY IMAGE MOTION
COMPONENT FOR BEACON AND STELLAR
CHANNEL, DETECTION OF LOW FREQUENCY
TRACKING SIGNATURE

METEOROLOGICAL DATA COLLECTION SYSTEM

SENSOR GROUPS FOR
TEMPERATURE (AIR, GROUND) - PRESSURE
HUMIDITY - TEMPERATURE GRADIENT
- WIND VELOCITY

DATA RECORDING & PROCESSING

OSCILLOSCOPE & CAMERA RECORDING of
SCINTILLATION WAVEFORMS

INTENSITY
FLUCTUATIONS
IMAGE
JITTER

{ • AUTO & CROSS CORRELATIONS
• POWER SPECTRAL DENSITIES
• CORRELATION WITH METEOROLOGICAL
DATA COLLECTION SYSTEM

Figure 51.   Atmospheric Scintillation and Image Jitter
Experiments - Spacecraft to Earth

This figure is a summary of the spacecraft transmitter and earth
receiver data for the up-looking atmospheric scintillation and image jitter
experiment. The required sensor groups for the meteorological data collec-
tion system are identified, and the data reduction and processing operations
which would follow the experiment are indicated.

56

EARTH TRANSMITTER DATA

*OPTICAL: .5145μ (LOW FREQUENCY MODULATED
TRACKING SIGNATURE)*

SPACECRAFT RECEIVER DATA

*OPTICAL: DETECTION of LASER BEACON
INTENSITY FLUCTUATION*

*MICROWAVE
TELEMETRY : SCINTILLATION DATA ENCODED
FOR REAL TIME RETURN
TRANSMISSION TO EARTH*

GROUND DATA RECORDING & PROCESSING

*OSCILLOSCOPE AND CAMERA RECORDING
of SCINTILLATION WAVEFORMS*

*INTENSITY
FLUCTUATION*
$\left\{\begin{array}{l} \cdot AUTO\ \& CROSS\ CORRELATIONS \\ \cdot POWER\ SPECTRAL \\ DENSITIES \end{array}\right.$

Figure 52. Atmospheric Scintillation Experiment -
Earth to Spacecraft

The earth transmitter and spacecraft receiver data for the down-
looking atmospheric scintillation experiment are shown. The required ground
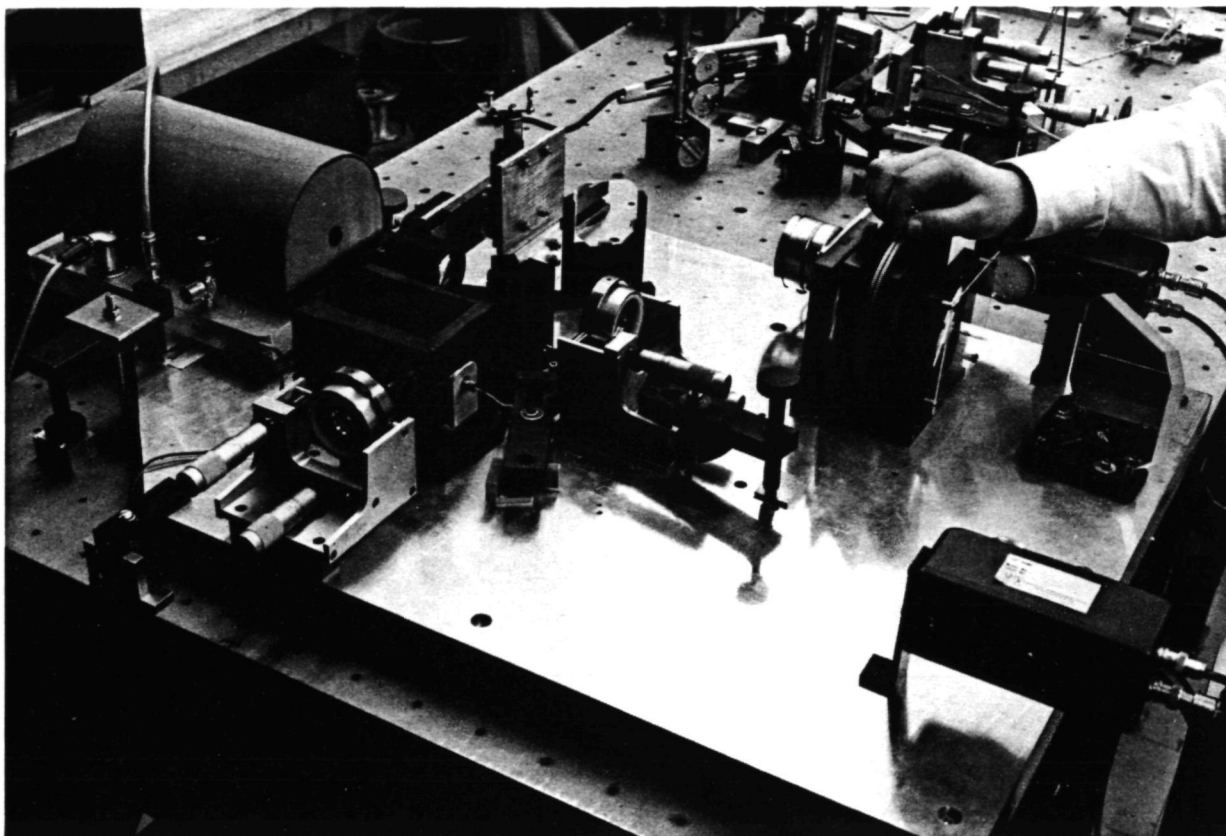data-processing operation is also indicated.

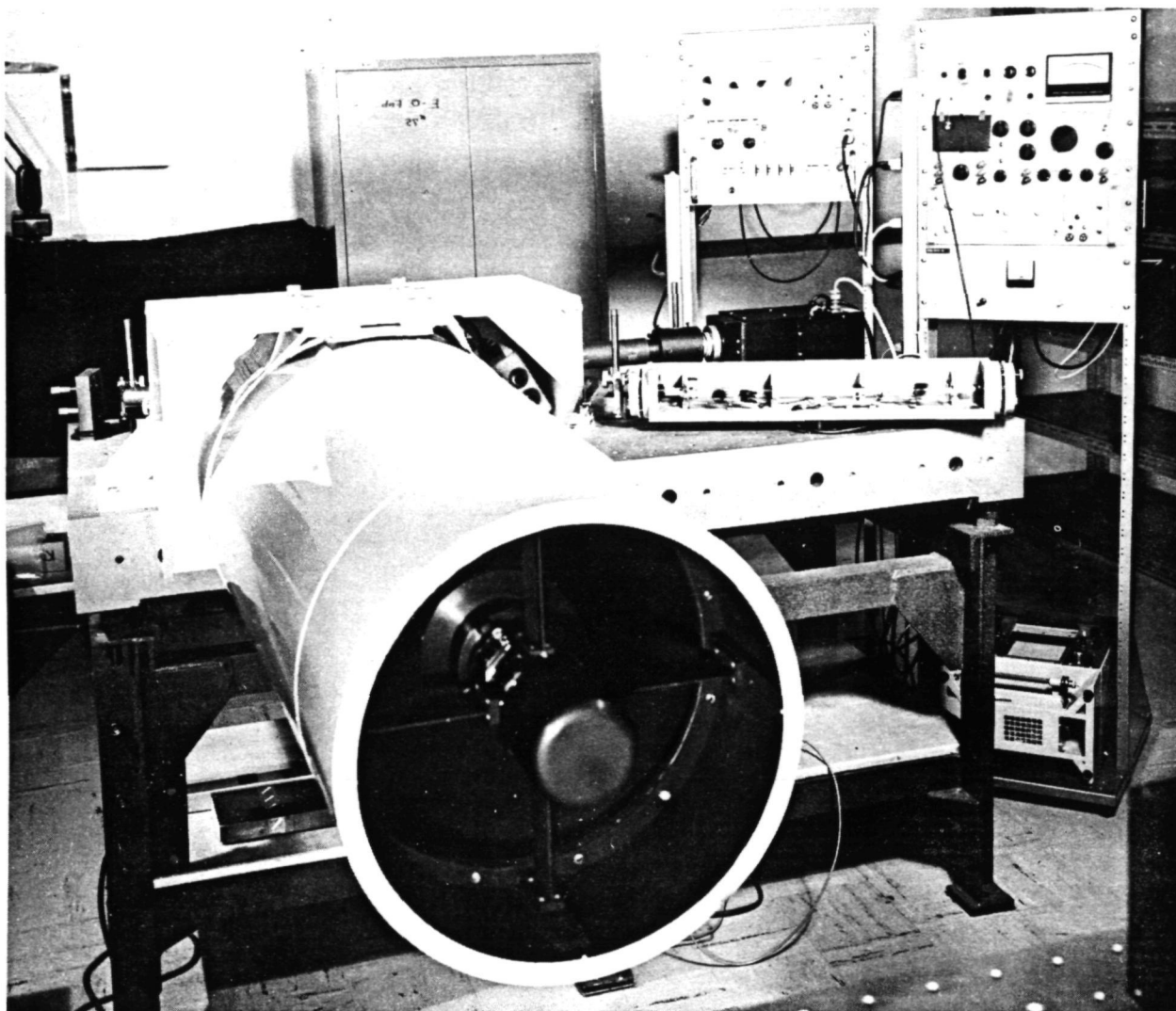Figure 53.   Phase Measuring Interferometer Apparatus Breadboard

Figure 54. Laser/Telescope Breadboard

The laser/telescope breadboard was used to demonstrate isolation between the 6328Å laser transmitter and the simulated 5145Å argon beacon and alignment between the laser transmitter and receive photomultipliers. For this demonstration, a cube corner image divider was located behind the telescope. Light from the laser was redirected back into the system, and the observer saw four images of varying intensity in the image plane. By adjusting the alignment of the laser transmitter, the intensity of the four images could be balanced indicating that the laser transmitter was at a conjugate focal point to the apex of the image dividing cube corner prism.